NASA TN D-1241

TECHNICAL NOTE

D-1241

EFFECTS OF SUCTION BOUNDARY-LAYER CONTROL ON THE PERFORMANCE OF A SHORT ANNULAR DIFFUSER WITH AN UPSTREAM TERMINAL NORMAL SHOCK

By Charles J. Shoemaker and John R. Henry

Langley Research Center
Langley Station, Hampton, Va.

NATIONAL AERONAUTICS AND SPACE ADMINISTRATION
WASHINGTON April 1962

60 p.

NATIONAL AERONAUTICS AND SPACE ADMINISTRATION

TECHNICAL NOTE D-1241

EFFECTS OF SUCTION BOUNDARY-LAYER CONTROL ON THE PERFORMANCE OF A SHORT ANNULAR DIFFUSER WITH AN UPSTREAM TERMINAL NORMAL SHOCK

By Charles J. Shoemaker and John R. Henry

SUMMARY

As part of a general program to determine methods for obtaining high performance in short subsonic diffusers for use with supersonic inlets, an investigation was conducted in which the effectiveness of suction boundary-layer control as a method for improving the performance of a short annular diffuser was evaluated. The equivalent conical expansion angle of the diffuser was 10°. A normal shock was positioned at distances ranging from 0.4 to 2.0 annulus gaps upstream from the diffuser entrance; the corresponding shock Mach number varied from 1.40 to 1.47. The boundary layer upstream of the normal shock occupied about 50 percent of the annular duct area, and boundary-layer suction flows as high as about 13 percent of the total diffuser entrance flow were employed.

Suction boundary-layer removal of about 5 percent of the total flow reduced the overall total pressure loss to values from 5 to 11 percent less than those for a 5° diffuser employing no boundary-layer control. For suction-flow rates from 5 to 8 percent, the total theoretical pumping power required to restore the suction flows and the diffuser exit flow to the total pressure upstream from the normal shock was no more than that required for the same diffuser exit mass flow with no boundary-layer control.

INTRODUCTION

The performance of the turbojet and ramjet propulsion systems in supersonic aircraft depends to a large extent on the performance of the air-induction system. One important component of the induction system is the terminal normal-shock duct and the subsonic diffuser. The severe adverse pressure gradients produced by the normal shock generally separate the boundary-layer flow, and a long constant-area duct or a very low-angle subsonic diffuser is required in order to recover the

normal-shock pressure rise (ref. 1). Either of these designs requires long lengths of ducting, and the aircraft performance is penalized by the added weight and space required.

The performance of an annular diffuser with a 10° equivalent expansion angle is presented for several lengths of normal-shock ducting and various amounts of suction boundary-layer control on both the inner and outer walls of the diffuser. The purpose of the investigation was to determine suction-flow quantities and relative pumping powers required in relation to improvements in performance for a reasonably short configuration. The performance of the configuration with no boundary-layer control is presented in reference 2.

The boundary layer in the throat of most supersonic inlets extends across the major portion of the throat area; therefore, for this investigation the ducting upstream from the diffuser entrance was made of sufficient length to produce thick boundary layers. A normal shock was positioned at distances ranging from 0.4 to 2.0 annulus gaps upstream of the diffuser entrance; the corresponding shock Mach number varied from 1.40 to 1.47. Up to about 13 percent of the mass flow was removed through suction openings in the diffuser walls. The Reynolds number based on the annulus gap at the entrance was 1.25×10^{6}.

SYMBOLS

a,b	substitution parameters given in appendix
A	cross-sectional-flow area
D	diameter
e	base for natural logarithms
$f_1\left(\frac{R_i}{R_o}\right)$ . . . $f_6\left(\frac{R_i}{R_o}\right)$	correlation factors given in appendix
m	mass flow, slugs/sec
M	Mach number
n	exponent in boundary-layer equation $\frac{u}{u_\delta} = \left(\frac{y}{\delta}\right)^{1/n}$
p	static pressure

Δp	static-pressure change
p_t	total pressure
Δp_t	total-pressure loss
$\overline{p_t}$	mass-weighted total pressure
P	net pumping-power coefficient
P_B	suction-flow pumping-power coefficient
R	boundary-layer suction mass flow, percent of total mass flow at the diffuser inlet
u	local velocity in boundary layer, ft/sec
u_δ	velocity at edge of boundary layer, ft/sec
x	axial distance measured downstream from the cylinder-diffuser junction (station 3a; see fig. 2)
Δx	increment of axial distance
y	radial distance
γ	ratio of specific heats
δ	boundary-layer thickness, in.
δ_i^*	displacement thickness of boundary layer on inner wall at station 3a for supersonic flow, $\frac{1}{2}\left(\sqrt{\frac{4\Delta_i^*}{\pi} + D_i^2} - D_i\right)$, 0.0584 in.
δ_o^*	displacement thickness of boundary layer on outer wall at station 3a for supersonic flow, $\frac{1}{2}\left(D_o - \sqrt{D_o^2 - \frac{4\Delta_o^*}{\pi}}\right)$, 0.0659 in.
δ_R^*	total displacement thickness of boundary layers at station 3a for supersonic flow, used as reference dimension for shock location, $\delta_i^* + \delta_o^*$, 0.1243 in.

Δ^* three-dimensional displacement area at station 3a, $\int_0^\delta \left(1 - \frac{\rho u}{\rho_\delta u_\delta}\right) dA$, sq in.

θ_3 three-dimensional momentum area at station 3a, $\int_0^\delta \frac{\rho u}{\rho_\delta u_\delta}\left(1 - \frac{u}{u_\delta}\right) dA$, sq in.

ρ mass density, slugs/cu ft

Subscripts:

c computed by one-dimensional theory

d downstream

i inner wall

N no suction and no suction openings

o outer wall

r suction reservoir

s at the shock location

t total

u upstream

δ located at edge of boundary layer

1,3,3a,6a,8 test-setup and diffuser stations (see figs. 1 and 2)

3-8 between stations 3 and 8

s-8 between shock location and station 8

max maximum

min minimum

opt optimum

A bar over a symbol indicates an average value.

APPARATUS AND PROCEDURE

General Apparatus

The test equipment (fig. 1) is the same as that described in reference 2 except for the addition of the suction boundary-layer control apparatus. The setup consisted of a 30-inch-diameter settling chamber with screens to reduce the turbulence of the flow, an annular-entrance venturi meter, a centerbody support section containing 18 struts of high fineness ratio, a supersonic nozzle section, the diffuser model and boundary-layer control ducting, an exit venturi meter, a section containing a butterfly control valve, and an exit diffuser. Since flow through small annuli in large-diameter ducting is approximately two dimensional, the supersonic nozzle was designed by using the two-dimensional, nonviscous characteristics method; the design Mach number was 1.6. The ducting had close tolerances with all joints smooth and sealed to prevent leaks.

L
4
1
9

Diffuser Model

The diffuser, which is the short configuration of reference 2, had a cylindrical outer wall with a diameter of 13.5 inches. (See fig. 2.) The centerbody shape was such that for about 83 percent of the diffuser length the flow area increase per unit length was the same as that of a 10° conical diffuser with the same entrance area and area ratio. The junction of the upstream end of the diffuser centerbody and the supporting cylinder consisted of a circular-arc contour. The terminal of the centerbody was an arbitrary fairing. These methods of design were used at the ends of the diffuser to avoid sharp changes in contour that would have been obtained from the area variation for an equivalent conical angle.

Boundary layer was removed by suction through three different hole patterns designated as four row, six row, and eight row. Each row had 20 holes equally spaced about the circumference of either the inner or outer wall of the diffuser. The four-row configuration consisted of two rows on both the inner and outer walls near the upstream end of the diffuser (fig. 2). The six-row configuration had an additional row on both the inner and outer walls located $15\frac{1}{2}$ inches from the upstream end of the diffuser. The eight-row configuration is shown in figure 2, which gives all hole sizes and locations. The open-hole area of the four-, six-, and eight-row configurations corresponded to 18, 21, and 24 percent, respectively, of the diffuser entrance area. The boundary-layer removal was accomplished by applying suction to the centerbody support duct for the inner wall and to the plenum chamber surrounding

the diffuser for the outer wall. The Reynolds number based on the annulus gap at the entrance to the diffuser was 1.25×10^6.

Instrumentation

A reference total-pressure tube and a thermocouple were located in the 30-inch-diameter settling chamber at station 1 (fig. 1). A longitudinal row of static-pressure orifices was placed on the diffuser inner wall opposite a similar row on the diffuser outer wall. Three static-pressure orifices were equally spaced circumferentially on the outer wall of the throat of the venturi meter at station 2 and in the throat of the venturi meter at station 8. (See fig. 1.) For the total-pressure surveys at stations 3a and 6a, three traversing tubes were used which were equally spaced circumferentially. (See fig. 2 for station locations.) Standard ASME orifice meters were placed in the boundary-layer suction ducts. The pressure readings of all static-pressure orifices were recorded by photographing multitube manometer boards. Total-pressure traverse data were recorded by using commercial transducer pressure cells with electronic data plotters, which limited the frequency response to 10 cycles or less and gave a continuous plot of pressure loss from a reference station to the survey position. The traverses were made to within 0.035 inch of each wall.

Test Procedure

The upstream venturi calibration of reference 2 was used to determine flow entering the diffuser. The results of total-pressure surveys at station 3, which are presented in reference 2, were used to determine the mass-weighted average total pressure of the supersonic flow at a location close to the diffuser inlet; this average pressure $\overline{p_{t,3}}$ was used as a reference pressure. Total-pressure surveys for several shock locations were made at station 3a, the cylinder-diffuser junction, to determine the diffuser inlet flow conditions in terms of total-pressure and Mach number distributions and boundary-layer parameters at the point where the duct area starts to increase. For these tests, the diffuser centerbody was replaced by a constant-diameter cylinder which extended the cylindrical centerbody well downstream from station 3a.

In the main series of tests in which the diffuser performance was measured, the initial steps consisted of locating the normal shock in a preselected position upstream from the diffuser entrance and setting preselected amounts of suction boundary-layer removal on the inner and outer walls. The location of the shock could be determined accurately by visual observation of a manometer which was connected to a series of wall static-pressure orifices. The shock was located at positions

ranging from 0.4 to 2.0 annulus gaps upstream from station 3a. The total amount of suction-flow removal ranged from 2.4 to 13.4 percent of the total flow at the diffuser inlet; the amount removed from each wall was regulated by use of control valves in the suction ducting. After positioning the normal shock and setting the suction flow, the static-pressure data were recorded photographically and the total-pressure traverses were made at station 6a.

Performance Comparison

The performances of the three configurations of boundary-layer bleed holes and the diffuser without bleed were compared by using the following performance parameters: overall total-pressure loss, total-pressure distribution at station 6a, static-pressure rise, and theoretical suction-flow pumping power. The overall total-pressure loss is defined as the difference between the mass-weighted average total pressure of the supersonic flow at station 3 and the total pressure at station 8. Since the flow distribution at station 8 was essentially one dimensional, the average total pressure was calculated from one-dimensional relations by using the measured static pressure at station 8 and the mass flows determined from the venturi-meter measurements at station 2 and the suction duct orifice plates. In comparing this overall total-pressure loss with theoretical values, it was corrected for the friction pressure loss of the supersonic flow between station 3 and the shock position. Total-pressure-loss and static-pressure-rise data have been nondimensionalized by referencing them to the mass-weighted total pressure at station 3 as was done in reference 2. The total-pressure-loss distributions at station 6a are presented as the loss in total pressure from station 1 to the survey point. The total pressure at station 1 was used because of the convenience in processing the data; however, the coefficient $\left(p_{t,1} - p_{t,6a}\right)/\overline{p_{t,3}}$ can be readily converted to $p_{t,6a}/\overline{p_{t,3}}$ by subtracting it from the quantity $p_{t,1}/\overline{p_{t,3}}$, which has a value of 1.104.

In order to evaluate the relative power required for boundary-layer removal, pumping powers were computed by methods similar to the procedures given in reference 3. It was assumed that an auxiliary pump of 100-percent efficiency would increase the pressure of each of the two suction flows from the pressures measured in the suction reservoirs to the total pressure just upstream from the normal shock. Also, the pump was assumed to increase the total pressure of the main flow at station 8 to that just upstream of the normal shock. These three pumping powers were added to produce a summation of pumping power required with suction-flow removal; the summation was divided by the pumping power with no suction flow to form a net pumping-power coefficient P, as illustrated by the following equation:

$$P = \frac{R_o\left[\left(\frac{p_{t,s}}{p_{t,ro}}\right)^{\frac{\gamma-1}{\gamma}} - 1\right] + R_i\left[\left(\frac{p_{t,s}}{p_{t,ri}}\right)^{\frac{\gamma-1}{\gamma}} - 1\right] + \left(1 - R_o - R_i\right)\left[\left(\frac{p_{t,s}}{p_{t,8}}\right)^{\frac{\gamma-1}{\gamma}} - 1\right]}{\left(1 - R_o - R_i\right)\left[\left(\frac{p_{t,s}}{p_{t,8}}\right)_N^{\frac{\gamma-1}{\gamma}} - 1\right]}$$

For no suction-flow removal, there was only the flow at station 8 to consider; however, the mass flow was assumed to be the same as that at station 8 with suction-flow removal on the assumption that the main flow or required engine airflow would be the same with or without suction boundary-layer control. A value of the coefficient P of 1.0 indicates that the net pumping power required to return the entire flow to its initial condition is exactly the same with or without suction boundary-layer removal when the main flow is considered to be the same for both cases.

The effects of certain variables on the suction pumping powers only were of interest; therefore, a suction-flow pumping-power coefficient P_B also was determined, which is defined as the summation of the pumping powers required for the two suction flows divided by the pumping power required with no suction-flow removal, as illustrated in the following equation:

$$P_B = \frac{R_o\left[\left(\frac{p_{t,s}}{p_{t,ro}}\right)^{\frac{\gamma-1}{\gamma}} - 1\right] + R_i\left[\left(\frac{p_{t,s}}{p_{t,ri}}\right)^{\frac{\gamma-1}{\gamma}} - 1\right]}{\left(1 - R_o - R_i\right)\left[\left(\frac{p_{t,s}}{p_{t,8}}\right)_N^{\frac{\gamma-1}{\gamma}} - 1\right]}$$

RESULTS AND DISCUSSION

Entrance Flow Conditions

Total-pressure and Mach number distributions of the flow entering the diffuser (at station 3a) are given in figure 3(a) for three normal-shock positions. The data represent averages of readings from the

three traversing rakes equally spaced about the circumference of the duct outer wall. With the shock downstream from the survey station (x_s/D_o of 0.208), the boundary layer occupied about 50 percent of the duct area, and the stream Mach number was about 1.5. The total displacement area for this condition was 6.7 percent of the duct area. (See table at top of figure.) The total displacement thickness δ_R^* corresponding to the displacement areas was 6.6 percent of the gap between the inner and outer walls or 0.92 percent of the outer diameter D_o. The inner-wall displacement thickness was 11.4 percent smaller than that for the outer wall. The ratios of displacement to momentum areas for both inner and outer walls were approximately 2.2; the corresponding values of the exponent n for the boundary-layer equation were between 7 and 8. These values are typical of a boundary layer which has not been subjected to an adverse pressure gradient.

L
4
1
9

As the shock was moved upstream to a position just in front of the survey station (x_s/D_o of -0.185), the boundary layers increased in thickness and became distorted. The data indicated some flow separation on the outer wall. The total displacement area increased to 20 percent of the duct area, the ratios of displacement to momentum area increased, and the boundary-layer exponent was reduced to values on the order of 1 to 2. These values are indications of a highly distorted boundary-layer distribution, which was produced by the abrupt pressure rise through the normal shock and the interaction effects of the shock on the boundary layer. As the shock was moved further upstream to an x_s/D_o position of -0.746, the boundary layers at station 3a thickened and improved in shape because of natural mixing of the flow between the shock position and the survey position.

The length of duct required to recover the pressure rise due to a normal shock is dependent on the relative thickness of the boundary layer at the shock. In addition, the performance of a subsonic diffuser is a function of the boundary-layer thickness at the entrance. Therefore, shock position will be given herein in terms of the total boundary-layer displacement thickness of the supersonic flow at station 3a. (See data for (x_s/D_o) of 0.208, fig. 3(a).) As mentioned previously, this displacement thickness δ_R^* is 0.92 percent of the outer diameter D_o.

The flow conditions at station 3a for the shock position corresponding to an x_s/D_o of -0.185 are of particular interest because this shock location is near the center of the range of shock positions covered by the test program (values of x_s/D_o ranging from -0.056 to -0.28). The information presented in figure 3(a) implies that the primary purpose of the suction boundary-layer control would be to correct the adverse effects imposed by the normal shock on the boundary layers in

order to obtain a more efficient subsonic diffusion. Figure 3(b), which is a mass-flow distribution corresponding to this shock location, illustrates the potential of suction boundary-layer removal. The portions of each boundary layer that would be removed by several values of suction flows are indicated. For instance, a total suction of 5.5 percent, composed of 2.5 percent on the inner wall and 3.0 percent on the outer wall corresponds to a value of about 0.55 for the ratio of local mass flow per unit area to average mass flow per unit area. Such suction-flow quantities would remove the lowest energy portions of the boundary layers, and significant improvements in performance might be anticipated. On the other hand, figure 3(b) shows that removal of the major portions of both boundary layers would require very high suction quantities which could not be justified by major improvements in performance.

The variation of shock Mach number with shock location is given in figure 4 for the three suction-row configurations used in the tests. The shock Mach number was computed by using one-dimensional relations, the average static pressure of the inner and outer walls at the shock location, and the mass flow measured in the venturi meter. The curves show that the Mach number generally decreases as the shock moves downstream. This decrease is attributed to friction total-pressure losses. The maximum scatter of the data is ±1.7 percent.

Longitudinal Distribution of Suction Mass Flow

The ratio of the mass flow through the upstream rows of holes to that through the downstream rows of holes was estimated for the inner and outer walls for the six- and eight-row configurations. In making the calculations, the assumption was made that the mass flow through a given row of holes is proportional to the square root of the product of the pressure at the exit of the holes and the pressure drop across the holes. The pressure at the entrance to the holes was determined from the wall static-pressure measurements in the diffuser, and the pressure at the exit of the holes was assumed to be equal to that measured in the suction reservoirs. The results of these computations are presented in figures 5 and 6 for the six-row and eight-row configurations, respectively. The ratio of upstream to downstream suction mass flow is given as a function of shock location and the total suction flow through the inner wall (figs. 5(a) and 6(a)) and through the outer wall (figs. 5(b) and 6(b)). The points are plotted for cases with and without separated flow in the diffuser, and families of curves of R_i or R_o are faired for the attached-flow cases. The separated-flow phenomena encountered in this investigation are discussed in more detail subsequently.

The figures show that there is nearly a linear relationship between the upstream-to-downstream mass-flow ratio and the total amount of suction flow for one wall. For six suction rows (fig. 5), the mass-flow ratio varies from about 2 to 4, depending on the total suction for the particular wall. Adding another row of holes (fig. 6) to the inner and outer walls reduced the ratio of upstream-to-downstream mass flow to values ranging from about 0.2 to 2.0, depending on the total suction for a given wall. It is evident that, within the limitations of the discrete hole patterns used, the configurations tested covered a wide range of longitudinal suction-flow distributions. Sufficient information is given in figure 5 for the six-row configuration and a shock position corresponding to an x_s/δ_R^* of -14.1 to determine that about 2.8 percent of the total flow was removed from a given wall in order to remove 2 percent of the total flow through the upstream rows of holes. Similarly, for the eight-row configuration (fig. 6), about 3.8 percent total-flow removal through a given wall was required to obtain 2.0 percent total-flow removal through the upstream rows of holes. Therefore, if it is assumed that a boundary-layer distortion should be removed near its origin, by implication the four-row configuration was most suited for control of boundary-layer disturbances originating at the normal shock, and the eight-row configuration furnished the most control for boundary-layer distortions occurring in the diffuser proper.

L 4 1 9

Diffuser-Exit Total-Pressure Distributions

Total-pressure traverses made at station 6a are presented in figures 7 to 10 as a function of the ratio of the cross-sectional area between the survey probe location and the inner wall to the total duct area at station 6a. An area ratio of 0.34 corresponds to the average annulus diameter. The ordinate scale has been inverted in order to make the plots resemble velocity distributions; relative velocity distributions may be determined with a maximum inaccuracy of a few percent by taking the square root of the difference between the total-pressure loss and static-pressure coefficients. The data have been divided into four groups in order to illustrate, within the limits of the available data, the effects of shock position, inner-to-outer-wall suction-flow ratio, total suction flow, and the number of suction rows.

Separated-flow phenomena.- In operating the test setup, it was impossible to regulate the amount of suction on the inner and outer walls in such a way that a smooth and continuous variation of the total-pressure distribution was obtained. For instance, if the total pressure at station 6a was high near the inner wall and low near the outer wall for a given operating condition, the inner-wall suction could be reduced or the outer-wall suction increased with consequent improvements in the distribution up to a certain limit. On reaching the limiting condition,

the flow would snap over to the outer wall and produce the reverse of the original distribution. The abrupt switch of the flow to the outer wall is believed to be the result of the attachment to the outer wall of the previously discussed separated flow and the separation from the inner wall of the boundary layer just downstream of the shock. The cases with separation on the inner wall produced lower performance values and are referred to herein as separated-flow cases. Data points corresponding to the relatively mild separation on the outer wall are identified for convenience as attached-flow points.

Shock position.- The effect of shock position on the total-pressure-loss distribution (fig. 7) is not significant for the ranges of suction flows given. For the eight-suction-row case (fig. 7(c)) when the shock was located 6.2 displacement thicknesses upstream from station 3a, the suction-flow quantities were such as to produce high total pressures near the outer wall and separated flow on the inner wall as previously discussed. A shock position slightly farther upstream (x_s/δ_R^* of -10.9) corresponded to the opposite flow pattern.

L
4
1
9

Inner-to-outer-wall suction-flow ratio.- The total-pressure-loss distribution was affected strongly by the relative amounts of suction flow through the inner and outer walls as illustrated by figure 8. As the ratio R_i/R_o was reduced, the distribution improved and the static pressure increased until a value was reached which produced the flow switch previously mentioned. When the flow switch occurred, the performance depreciated; this phenomenon indicates the existence of optimum values of R_i/R_o which are discussed subsequently.

Total suction-flow quantity.- Increases in the overall suction rate (fig. 9) did not generally produce a significant change in the distribution, providing the flow did not switch from one wall to the other. An exception to this statement is illustrated in figure 9(c), where increasing the total suction flow from 7.35 percent to 11.33 percent shifted the location of the peak total pressure and changed the distribution somewhat.

Hole pattern.- Changing the hole pattern produced some changes in the total-pressure distribution, as shown in figure 10. Shifting the suction-flow removal upstream (decreasing the number of rows of holes) tended to flatten the distribution and shift the peak towards the inner wall. Figure 10 also shows a very large favorable effect on the distribution due to suction as compared with no boundary-layer control.

Diffuser-Exit Total-Pressure Distortion

Some of the detailed differences to be noted in the total-pressure-loss distributions of station 6a can be determined more accurately

through the use of the total-pressure distortion factor which, for a given distribution, is defined as the ratio of the difference between the maximum and minimum total pressures at station 6a to the average total pressure at station 3. The minimum total pressure by definition is taken at a point separated from the wall by 5 percent of the duct cross-sectional area. This procedure allows for the existence of a certain amount of boundary layer outside of the region accounted for by the distortion factor. The total-pressure distortion factors for the tests with boundary-layer control are presented in figure 11 as a function of the inner-to-outer-wall suction-flow ratio. The separated-flow cases, for which the minimum total-pressure point occurred near the inner wall, produced considerably higher distortion factors than the attached-flow cases. The inner-to-outer-wall suction-flow ratio produced a strong effect for the attached-flow cases, as shown by the faired curves. The faired curves also show a favorable effect due to increasing the total suction flow. Shock locations close to the diffuser inlet produced higher distortions (fig. 11(c)), and the effect of inner-to-outer-wall suction ratio was diminished by movement of the shock upstream. The four-row configuration produced the lowest distortions; for instance, the value of total-pressure distortion was about 0.07 for a shock position x_s/δ_R^* of -6.05 and a total suction flow R_t of 6.3 percent.

Overall Total-Pressure Loss

Effects due to suction flow and shock position.- Because of the large number of independent variables for this investigation, the complete mapping of the individual effects of each parameter was not feasible. Therefore, in presenting the data, approximate correlation methods were utilized to determine empirical relations which fit the data. These relations were then used to compute curves showing the effects of the various parameters. The correlation of the overall total-pressure loss is presented in the appendix.

The effect of suction boundary-layer control on the overall total-pressure-loss coefficient, as computed from the equations of the appendix, is illustrated in figure 12 for suction flows up to 12 percent and for the several shock positions and suction-row configurations. The calculations were performed for the optimum values of the ratio of inner-to-outer-wall suction flow and also for values of R_i/R_o which are 10 percent larger than optimum. The definition of the optimum R_i/R_o is given in the appendix. The larger value of R_i/R_o is of interest because an operating condition should have some margin of separation from a flow condition corresponding to incipient boundary-layer detachment. The amount of increase in loss coefficient chargeable to this

10-percent margin varies with shock position, suction-row configuration, and the amount of suction, as shown in figure 12.

The loss coefficient is nearly a linear function of total suction-flow rate R_t for values of R_t greater than 2 percent. (See fig. 12.) The curves of each of the plots are nearly all parallel; this result indicates that shock position did not have a large effect on the reduction in loss coefficient due to suction. The figure also shows that the optimum suction-row configuration varies with the amount of total suction flow.

Breakdown of overall total-pressure loss.- In order to determine more precisely the relative advantages of suction boundary-layer control, the various factors which contribute to the total-pressure loss have been determined, and the results are plotted on figure 13 for suction-flow rates of 5 and 10 percent. Data for no suction boundary-layer control from reference 2 and curves for the suction data corresponding to correlation values for optimum R_i/R_o are presented. The loss coefficient has been modified from that previously discussed and is defined as the loss in total pressure to station 8 from a point just upstream from the normal shock divided by the average total pressure at station 3. The conversion of the upstream total-pressure reference from station 3 to each shock position was made by using computed values of the friction losses in the supersonic flow between station 3 and the shock positions. Equations (6) and (7) from reference 4 and the friction factor for smooth pipe given in reference 5 were employed. The maximum friction loss computed was 2.7 percent of the total pressure at station 3, and this maximum value was for the most downstream shock position. The data for no boundary-layer control given in figure 13 are slightly lower than corresponding values in reference 2 due to an error in processing the data of reference 2. The maximum discrepancy is 8 percent of the total-pressure loss.

Curves for the theoretical (one-dimensional) normal-shock loss with and without the addition of the "normal" subsonic diffuser loss are given for comparison purposes. The normal-shock loss was computed by using the measured values of shock Mach number. The "normal" subsonic diffuser loss was derived by using the subsonic test data of reference 2 and assuming that the Mach number at the diffuser inlet would be the theoretical Mach number downstream from the normal shock. The curves representing the summation of the two theoretical total-pressure losses (reference loss curves) correspond to a lower limit for the loss coefficient for which the normal shock exerts no influence on the subsonic diffusion.

As discussed in reference 2, the differences between the measured total-pressure losses and the reference loss curve were considered to

be produced by the influence of the normal shock on the subsonic diffusion and have been designated as shock—boundary-layer interaction losses. The curves of measured loss coefficient for the 10° diffuser with no boundary-layer control reach a minimum at a shock position of about 50 reference displacement thicknesses upstream from the diffuser inlet. Thus, for this condition the length of duct between the shock and the diffuser inlet was sufficient to minimize the shock—boundary-layer interaction losses. The curves of figure 13(a) indicate that with boundary-layer removal corresponding to 5-percent suction flow, the shock—boundary-layer interaction losses were reduced by about 50 percent. The configuration with four rows of holes produced the best performance and had loss coefficients at all shock positions which were less than the minimum value for the 10° diffuser with no boundary-layer control. Furthermore, the loss coefficients of the four-row configuration were from 5 percent to 11 percent less than those for the 5° diffuser with no boundary-layer control. This result indicates that the 5° diffuser, which is undesirably long, can be replaced with the 10° diffuser and 5-percent suction boundary-layer removal with no reduction in performance in terms of total-pressure loss.

With 10-percent suction flow (fig. 13(b)), the shock—boundary-layer interaction losses were reduced from 50 to 90 percent, depending on the shock location. In this case the configuration with six suction rows produced the lowest total-pressure losses over most of the range of shock positions.

Static-Pressure Rise

Longitudinal static-pressure distributions.- Typical longitudinal static-pressure distributions along the inner wall are presented in figure 14 for the three configurations of suction rows. Each plot illustrates several shock locations, and both attached- and separated-flow cases are included. Each distribution is characterized by an initial, nearly constant static-pressure region corresponding to the upstream supersonic flow, a sharp pressure rise at the normal-shock location, an additional rapid pressure rise at the location of the upstream rows of suction holes, and a gradual pressure rise due to the subsonic diffusion. In many cases the pressure rise at the location of the downstream rows of suction holes is hardly detectable because of the low velocities in the duct at this location. Details of the longitudinal distributions are analyzed subsequently.

Duct lengths required to recover theoretical static-pressure rise.- The theoretical static-pressure rise through the normal shock and the diffuser is presented in figure 15 for the three configurations of suction rows and several shock positions. The static pressure on the inner wall at the shock location was obtained from the data for points

as near the optimum inner-to-outer-wall suction-flow ratio as the data permitted and for points corresponding to a total suction flow of approximately 7 percent. The shock Mach numbers obtained from the data were used to compute normal-shock pressure rise, which was added to the initial pressure to produce the curves for pressure ratio downstream from the shock. Finally, the isentropic subsonic diffuser pressure rise due to the area change and the amount of boundary-layer removal was computed and added to the pressure downstream from the shock to produce the overall pressure-ratio curves at the top of figure 15.

The theoretical static-pressure-rise values of figure 15 were used in combination with the longitudinal distributions illustrated in figure 14 to determine the lengths of duct required to recover certain fractions of the theoretical static-pressure rise; duct length is defined as the distance from the normal-shock location to some point in the diffuser. The results are presented in figure 16, which shows duct length as a function of shock location for the three configurations of suction rows. Data from reference 2 for no boundary-layer control are included for comparison. The curves for boundary-layer control have a random shape because the total suction flow was not exactly the same for all shock positions and because the ratio of inner-to-outer-wall suction flow was not exactly optimum. However, some observations may be made from the general level of the curves.

L
4
1
9

The configurations with four and six suction rows required the shortest duct lengths for a given pressure rise. As high as 94 percent of the theoretical static-pressure rise was recovered at the centerbody terminal (six suction rows; x_s/δ_R^* of -14.9; R_t = 7.09 percent). The theoretical normal-shock pressure rise was obtained at a position just slightly downstream from the second row of suction holes. Comparison of the best suction-row configurations with the data for no boundary-layer control indicates that suction saved duct lengths up to $0.17D_o$ for the most upstream shock positions $\left(x_s/\delta_R^* \text{ of } -30\right)$; however, for shock positions close to the diffuser inlet, duct lengths as high as $1.3D_o$ were saved by the use of suction boundary-layer control. The latter refers to a comparison of the no-suction data with the four-suction-row configuration for a shock position x_s/δ_R^* of -7 and about 6.3-percent suction. In order to recover 70 percent of the theoretical static-pressure rise, a duct length of $1.89D_o$ was required without suction, but with suction only 33 percent of this length ($0.63D_o$) was required.

Pumping Power

Suction pumping-power coefficient.- The coefficient P_B, which is defined as the ratio of pumping power required for the suction mass flow

divided by the pumping power required with no boundary-layer control and the same mass flow at station 8 as with suction, is presented in figure 17 as a function of the total suction flow and the shock position. The data show that for a given amount of suction, the upstream shock locations corresponded to somewhat smaller coefficients than the downstream positions except for the six-row configuration, where shock location had little effect on the pumping-power coefficient. The plot showing the comparison of the three configurations of suction rows emphasizes the advantage, relative to pumping power, of increasing the total bleed-hole area.

Net pumping-power coefficient.- The net pumping-power coefficient P which is defined as the sum of the bleed pumping power and the main flow pumping power divided by the pumping power with no boundary-layer control and the same mass flow at station 8 as with suction, was correlated in a manner analogous to the total-pressure-loss correlations, and the results are presented in the appendix. The empirical equations of the appendix were used to compute the net pumping-power coefficient as a function of the total percent suction for optimum ratios of inner-to-outer-wall suction flows, and the results are given in figure 18.

The data show that for no additional cost in relative pumping power (a value of P of 1.0), bleed flows from 5 to 8 percent can be used, depending on the row configuration and shock position. For a given amount of suction flow, the shock position did not have a large effect on the coefficient except for the eight-suction-row configuration at total suction rates above about 8 percent. Increasing the number of suction rows tended to decrease the value of net pumping coefficient.

The results of figure 18 are further illustrated in figure 19, where P is presented as a function of shock position for 5- and 10-percent suction flows. The trend is for the net coefficient to increase as the shock is moved upstream except for the eight-suction-row case for 10-percent suction. It should be noted that all the 5-percent suction cases represent savings in relative pumping power.

SUMMARY OF RESULTS

The performance of an annular diffuser with a 10° equivalent expansion angle was determined for entrance flow conditions simulating those at the throat of a supersonic inlet. A normal shock was positioned at distances ranging from 0.4 to 2.0 annulus gaps upstream from the diffuser entrance; the corresponding shock Mach number varied from 1.40 to 1.47. Suction boundary-layer control was utilized by removing up

to about 13 percent of the total mass flow through rows of holes in the diffuser walls. The boundary layer upstream of the normal shock occupied about 50 percent of the annular duct area. The following significant results were obtained:

1. Pressure surveys at the diffuser entrance station indicated that the total boundary-layer-displacement thickness upstream from the normal shock was equal to 6.6 percent of the gap between the inner and outer walls, and that the boundary layer on the outer wall downstream from the normal shock was separated.

2. The value of the ratio of suction mass flow through the inner wall to that through the outer wall was critical. If the ratio was reduced below an optimum value, the boundary layer detached from the inner wall, and there was a depreciation in performance.

3. Pressure surveys at a station near the diffuser exit indicated that for a normal-shock position close to the diffuser entrance (6.05 displacement thicknesses upstream), total-pressure distortion factors as low as 0.07 were obtained by approximately 6-percent suction-flow removal.

4. For all normal-shock locations, the overall total-pressure loss from a point just upstream from the normal shock to a point in the duct downstream from the diffuser exit was reduced with 5-percent suction boundary-layer removal to values from 5 percent to 11 percent less than those for a 5° diffuser employing no boundary-layer control.

5. For suction-flow rates from 5 to 8 percent, the total theoretical pumping power required to restore the suction flows and the diffuser exit flow to the total pressure upstream from the normal shock was no more than that required for the same diffuser exit mass flow with no suction boundary-layer control.

6. Longitudinal wall static-pressure measurements indicated that 7-percent suction boundary-layer removal produced a static pressure at the diffuser exit equivalent to as high as 94 percent of the theoretical static-pressure rise through the normal shock and subsonic diffuser. For a normal-shock location close to the diffuser entrance and for no boundary-layer suction, 70 percent of the theoretical static-pressure rise was recovered at the diffuser exit; with about 6.3-percent suction boundary-layer removal, the same relative pressure rise was obtained within 33 percent of the duct length required without suction.

Langley Research Center,
National Aeronautics and Space Administration,
Langley Air Force Base, Va., February 1, 1962.

APPENDIX

EMPIRICAL DATA CORRELATIONS

Overall Total-Pressure Loss

Figure 20 illustrates empirical correlations applying to the overall total-pressure-loss coefficient, $\frac{\overline{p_{t,3}} - p_{t,8}}{\overline{p_{t,3}}} \equiv \frac{\Delta p_t}{\overline{p_{t,3}}}$, for the three configurations of suction rows. The ordinate of each figure indicates a correlation factor which corresponds to the following empirical relations:

For four suction rows,

$$\left(\frac{\Delta p_t}{\overline{p_{t,3}}}\right)_N - \left(\frac{\Delta p_t}{\overline{p_{t,3}}}\right) = \left[f_1\left(\frac{R_i}{R_o}\right)\right]\left\{0.0165 + 0.00507\left[1.30 - 0.0332\left(\frac{-x_s}{\delta_R^*}\right)\right]^{4.24}\right\} R_t^{0.337}$$

For six suction rows,

$$\left(\frac{\Delta p_t}{\overline{p_{t,3}}}\right)_N - \left(\frac{\Delta p_t}{\overline{p_{t,3}}}\right) = \left[f_2\left(\frac{R_i}{R_o}\right)\right]\left[0.00938 - \frac{0.1185}{1,000}\left(-\frac{x_s}{\delta_R^*}\right)\right] R_t^{0.794}$$

For eight suction rows,

$$\left(\frac{\Delta p_t}{\overline{p_{t,3}}}\right)_N - \left(\frac{\Delta p_t}{\overline{p_{t,3}}}\right) = \left[f_3\left(\frac{R_i}{R_o}\right)\right]\left(a + bR_t^{1.33}\right)$$

where

$$a = \left[\frac{0.0902}{\left(-\frac{x_s}{\delta_R^*}\right)^{0.537}} - 0.004\right]\left(1 - \frac{1}{e^{1.4R_t}}\right)$$

and

$$b = \left[0.960 - \frac{1.820}{\left(-\frac{x_s}{\delta_R^*}\right)^{1.11}}\right]\frac{1}{10^3}$$

Since the correlation factors apply to the attached-flow data only, the points in figure 20 for separated flow have a random scatter. Figure 20 lists estimates of minimum and optimum values of the inner-to-outer-wall suction-flow ratio for attached flow and values of the loss coefficients for no boundary-layer control used in the correlations. The optimum inner-to-outer-wall suction-flow ratio is defined as the ratio estimated to correspond to the minimum overall loss coefficient with attached flow. Within the accuracy of the data the optimum value was independent of the total suction flow and only a function of shock position and suction-row configuration. In general, the optimum value of R_i/R_o is the minimum value obtainable with attached flow; the numerical values presented were obtained by interpolation between the data point with the lowest R_i/R_o with attached flow and the next closest data point for separated flow. One exception is noted in figure 20(a) for four suction rows and a value of x_s/δ_R^* of -30.15, where the correlation curve peaks and the optimum value of R_i/R_o is 0.84 and the minimum value for attached flow is 0.52. The correlations of attached-flow data points of figure 20 indicate a maximum inaccuracy of about ±2 percent of the total-pressure loss.

Net Pumping-Power Coefficient

Figure 21 illustrates empirical correlations applying to the net pumping-power coefficient. The following relations were obtained:

For four suction rows,

$$P = \left[f_4\left(\frac{R_i}{R_o}\right)\right]\left[0.762\left(-\frac{x_s}{\delta_R^*}\right)^{0.0361} e^{0.00566R_t^2}\right]$$

For six suction rows,

$$P = \left[f_5\left(\frac{R_i}{R_o}\right)\right]\left[0.769\left(-\frac{x_s}{\delta_R^*}\right)^{0.0525} e^{0.00337R_t^2}\right]$$

For eight suction rows,

$$P = \left[f_6\left(\frac{R_i}{R_o}\right)\right]\left(0.0592\left\{1 + 0.446\left[1 - 0.0332\left(\frac{-x_s}{\delta_R^*}\right)\right]^{2.47}\right\}R_t\right) + 0.707\left\{1 - 0.652\left[1 - 0.0332\left(\frac{-x_s}{\delta_R^*}\right)\right]^{2.77}\right\}$$

For attached flow the maximum deviation of the data points from the faired curves is about ±3 percent.

REFERENCES

1. Shapiro, Ascher H.: The Dynamics and Thermodynamics of Compressible Fluid Flow. Vol. II. The Ronald Press Co., c.1954, pp. 1153-1156.

2. Wood, Charles C., and Henry, John R.: Effects of Shock—Boundary-Layer Interaction on the Performance of a Long and a Short Subsonic Annular Diffuser. NACA RM L58A31, 1958.

3. Wilbur, Stafford W., and Higginbotham, James T.: Investigation of Two Short Annular Diffuser Configurations Utilizing Suction and Injection as a Means of Boundary-Layer Control. NACA RM L54K18, 1955.

4. Henry, John R.: One-Dimensional, Compressible, Viscous Flow Relations Applicable to Flow in a Ducted Helicopter Blade. NACA TN 3089, 1953.

5. Henry, John R.: Design of Power-Plant Installations. Pressure-Loss Characteristics of Duct Components. NACA WR L-208, 1944. (Formerly NACA ARR L4F26.)

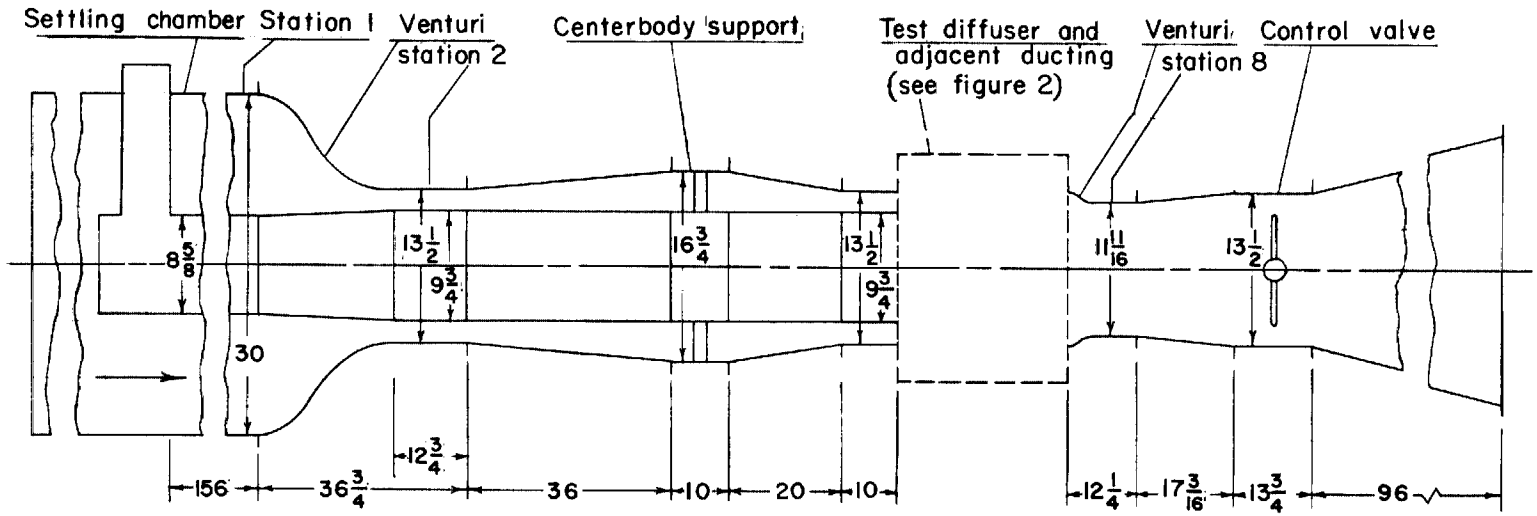

Figure 1.- Diagram of test setup. All dimensions are in inches.

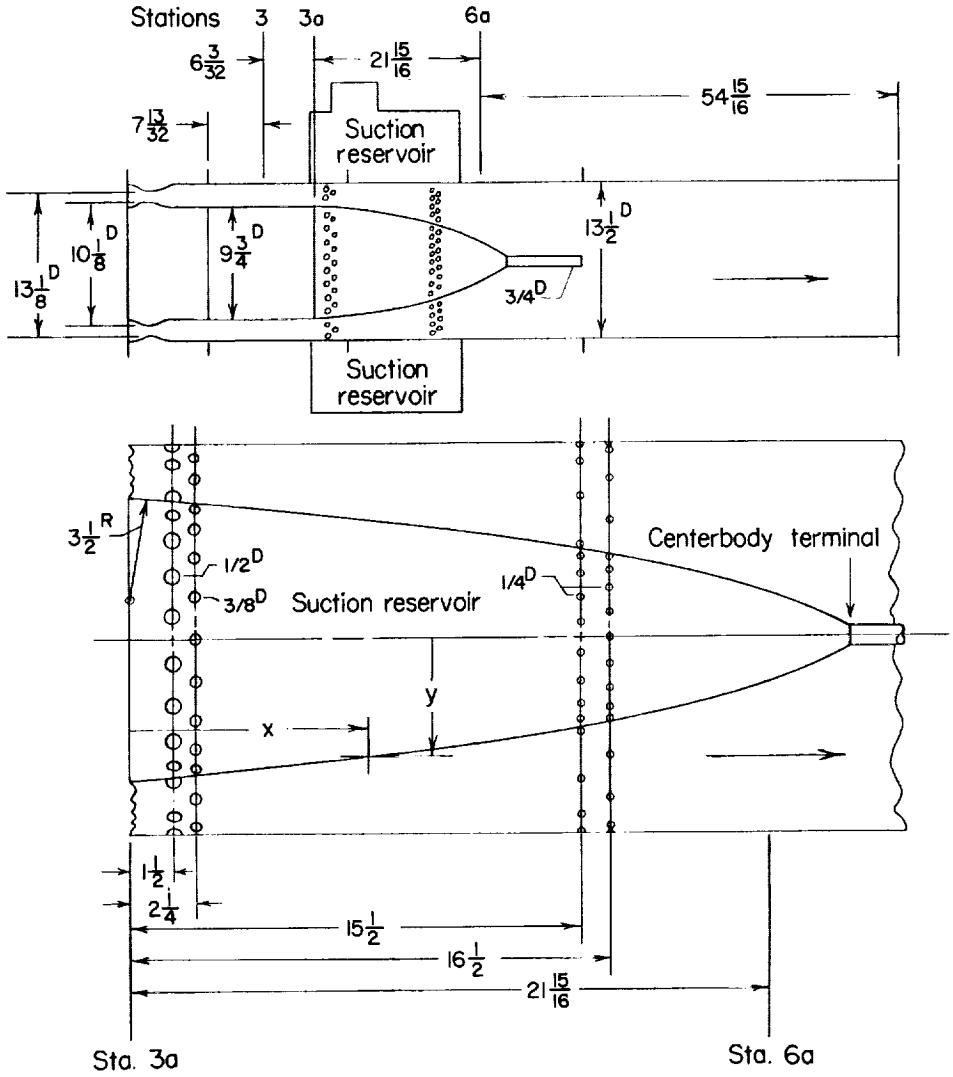

Coordinates for 10° diffuser

x	y	x	y
0.0	4.875	14.250	3.291
.062	4.875	18.250	2.565
2.250	4.701	22.250	1.445
4.250	4.514	23.250	1.040
6.250	4.312	25.350	.0
10.250	3.851		

Figure 2.- Diagram of diffuser model and ducting contained within the dashed-line section in figure 1. All dimensions are in inches.

$\frac{x_s}{D_o}$	$\left(\frac{\Delta^*}{A_t}\right)_i$	$\left(\frac{\Delta^*}{A_t}\right)_o$	$\left(\frac{\Delta^*}{\theta_3}\right)_i$	$\left(\frac{\Delta^*}{\theta_3}\right)_o$	n_i	n_o
.208	.026	.041	2.19	2.21	7.7	7.3
−.185	.067	.134	2.64	4.03	2.1	1.4
−.746	.047	.067	1.58	1.50	7.0	8.3

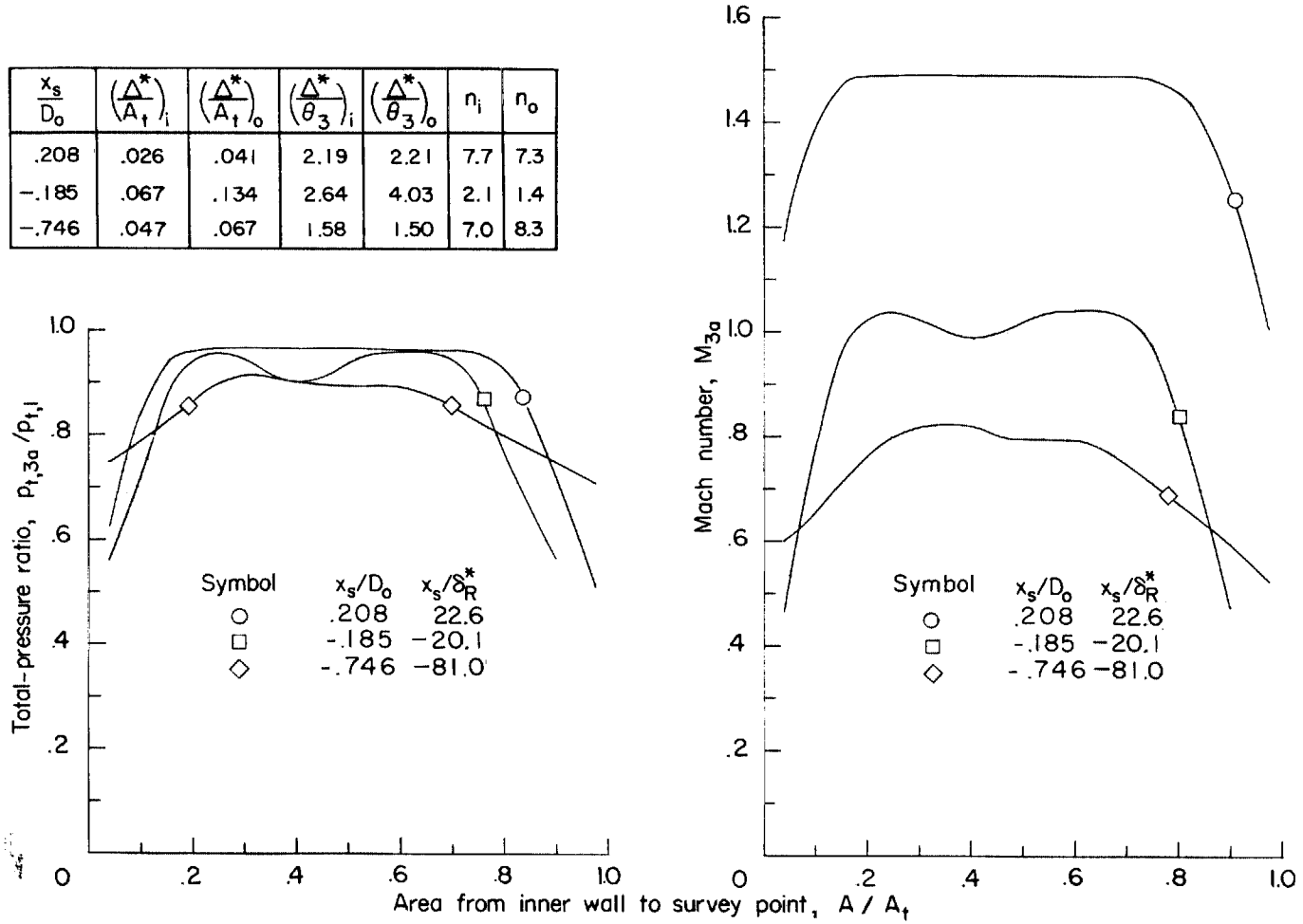

(a) Total-pressure ratio and Mach number distributions for several shock positions. Symbols on curves do not represent test points, but are used merely to identify the curves.

Figure 3.- Flow conditions at the cylinder-diffuser junction, station 3a.

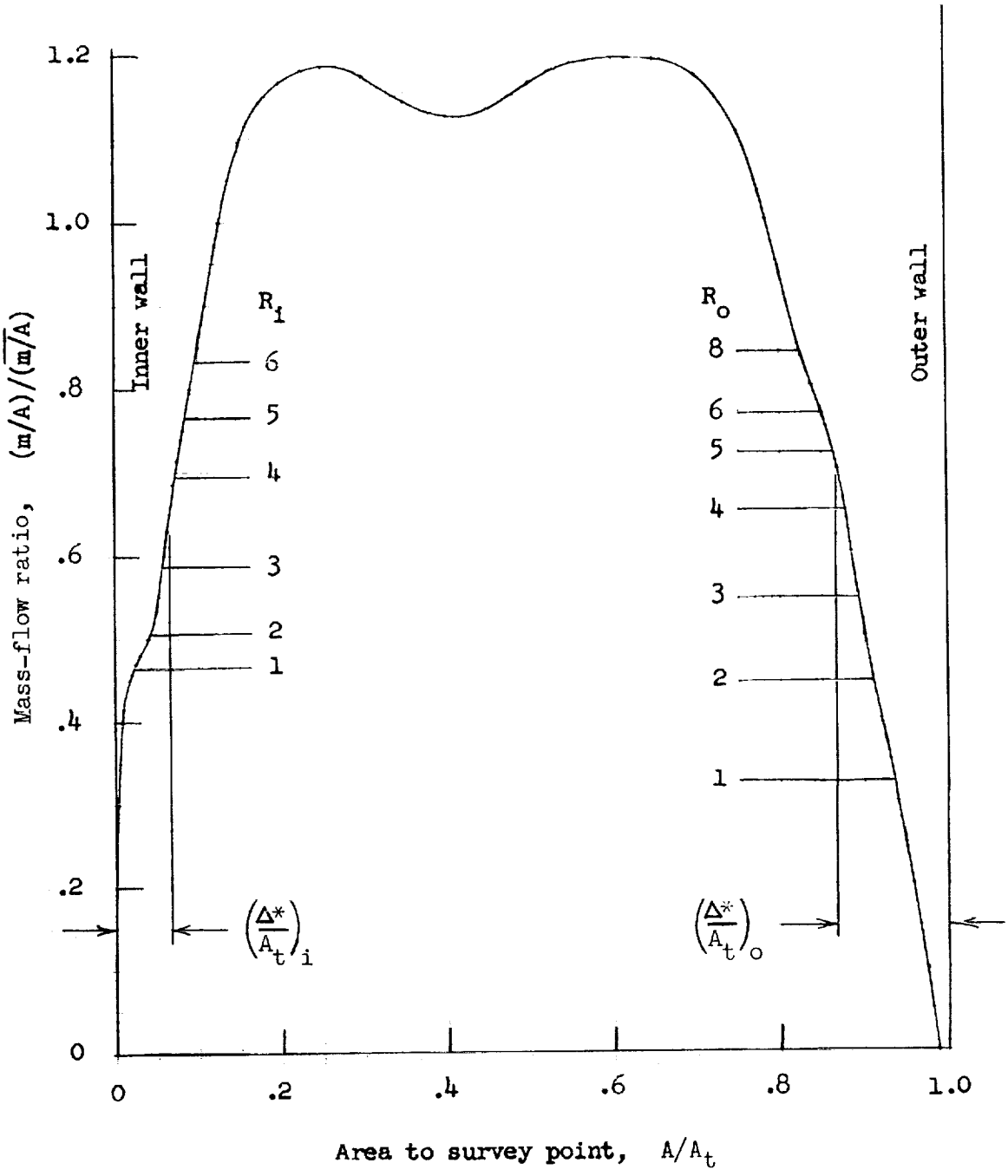

(b) Mass-flow distribution for a shock location x_s/D_o of -0.185.

Figure 3.- Concluded.

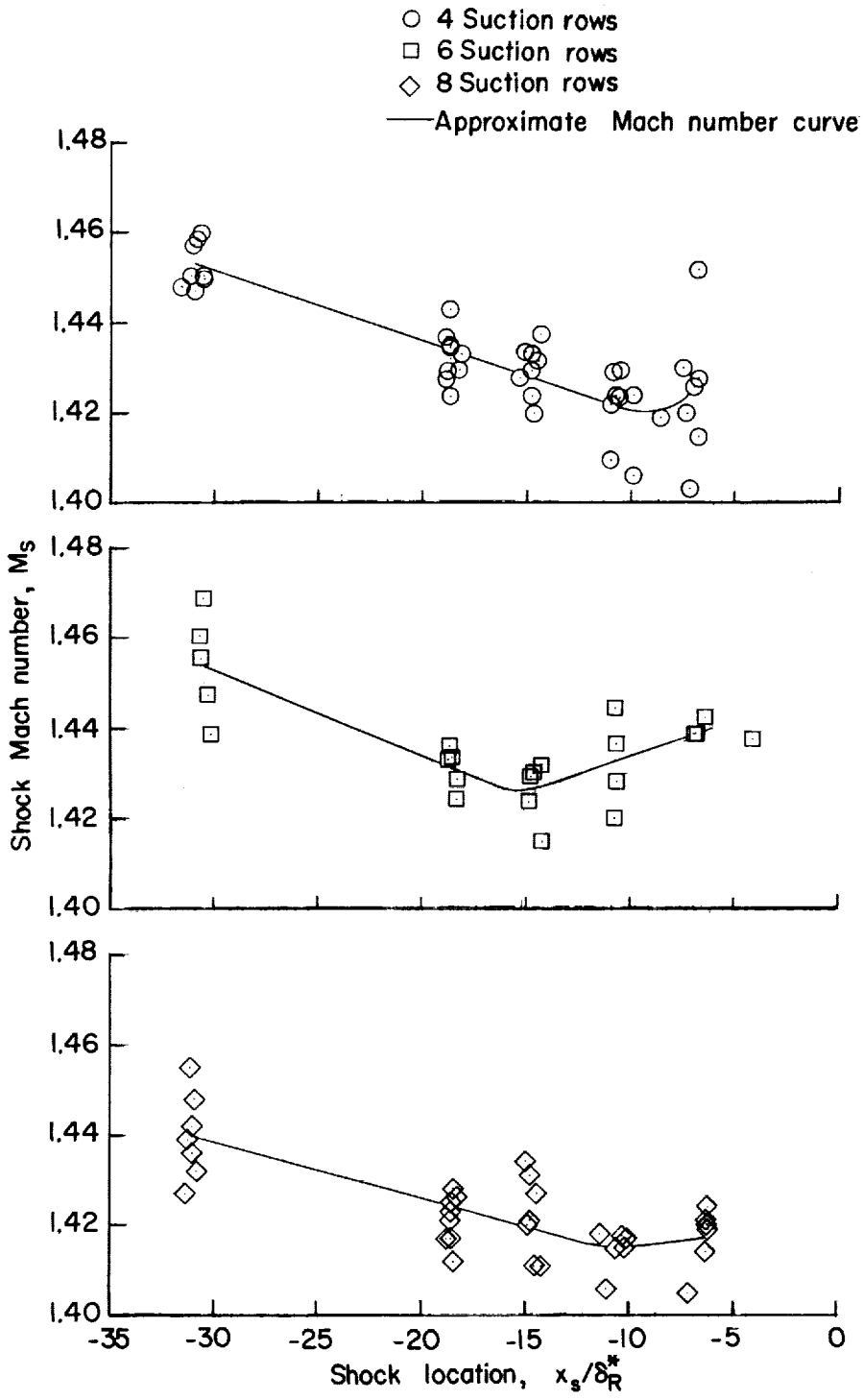

Figure 4.- Variation of shock Mach number with shock location.

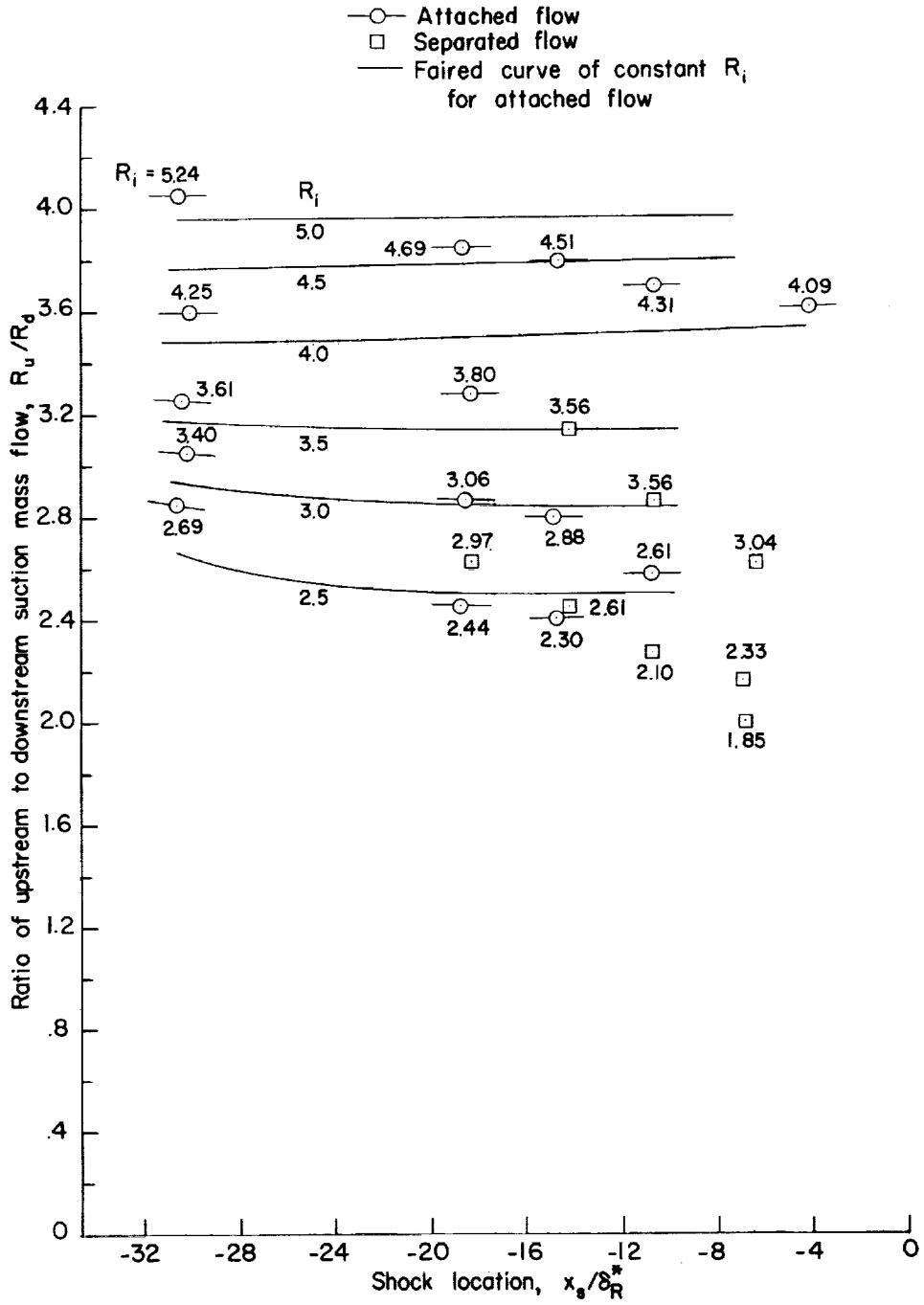

(a) Inner wall.

Figure 5.- Ratio of upstream to downstream suction mass flows for six-row configuration at several shock locations.

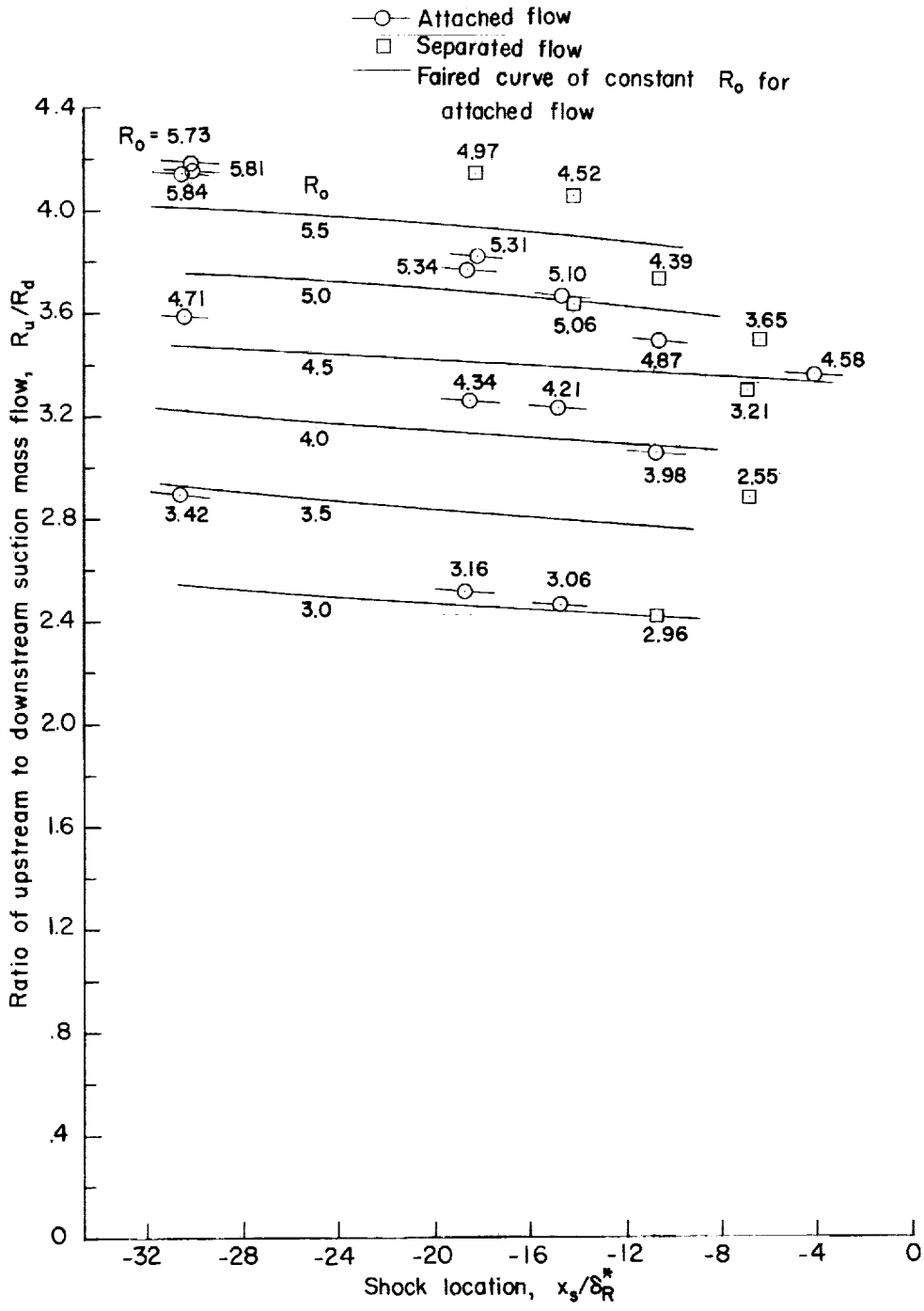

(b) Outer wall.

Figure 5.- Concluded.

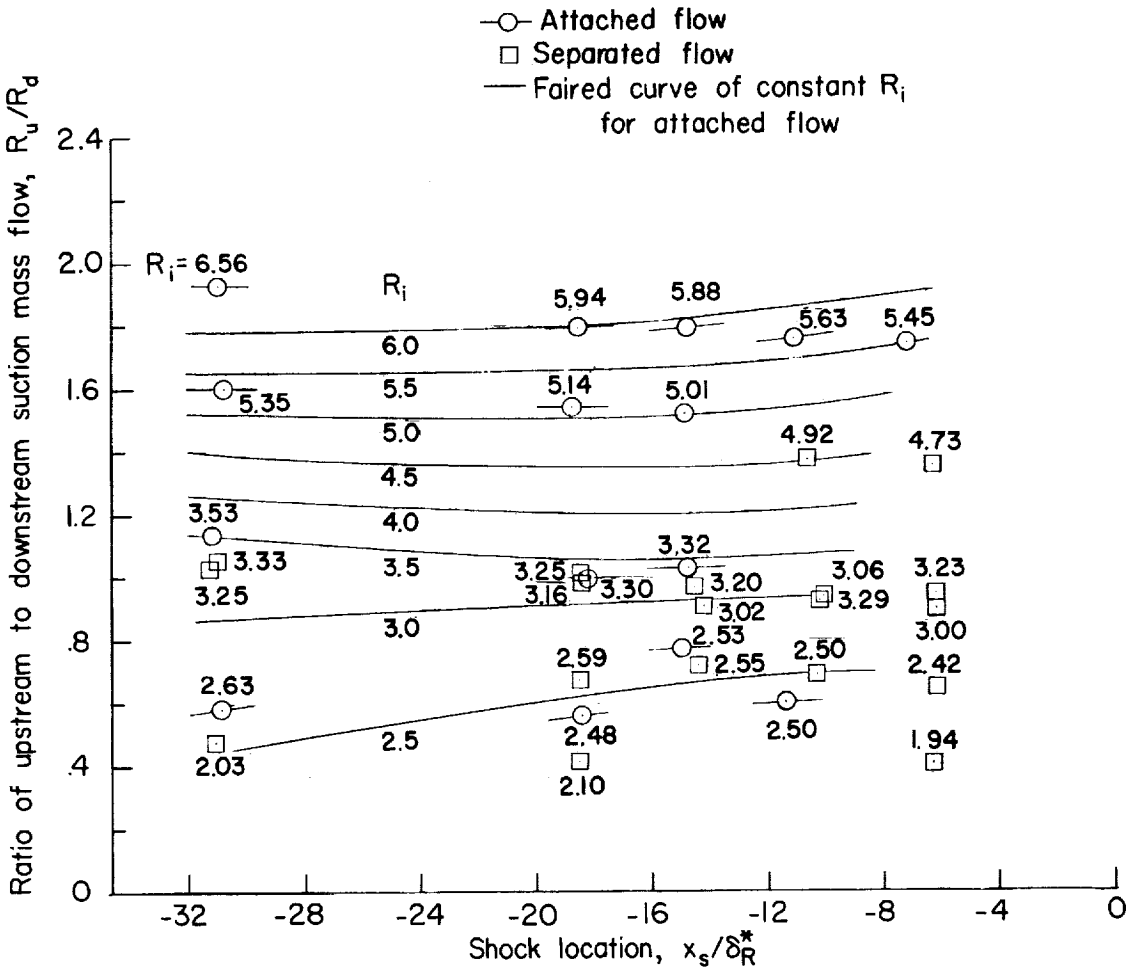

(a) Inner wall.

Figure 6.- Ratio of upstream to downstream suction mass flows for eight-row configuration at several shock locations.

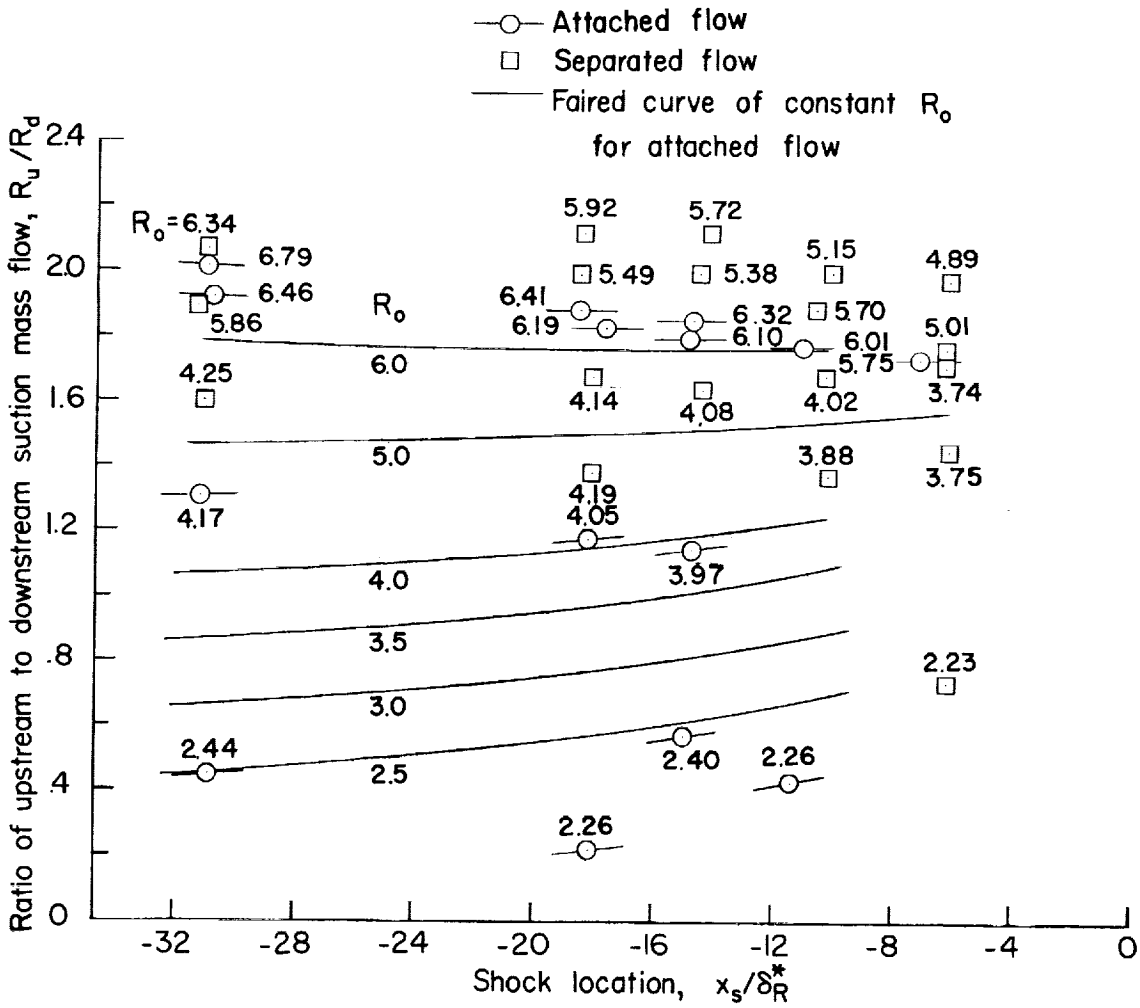

(b) Outer wall.

Figure 6.- Concluded.

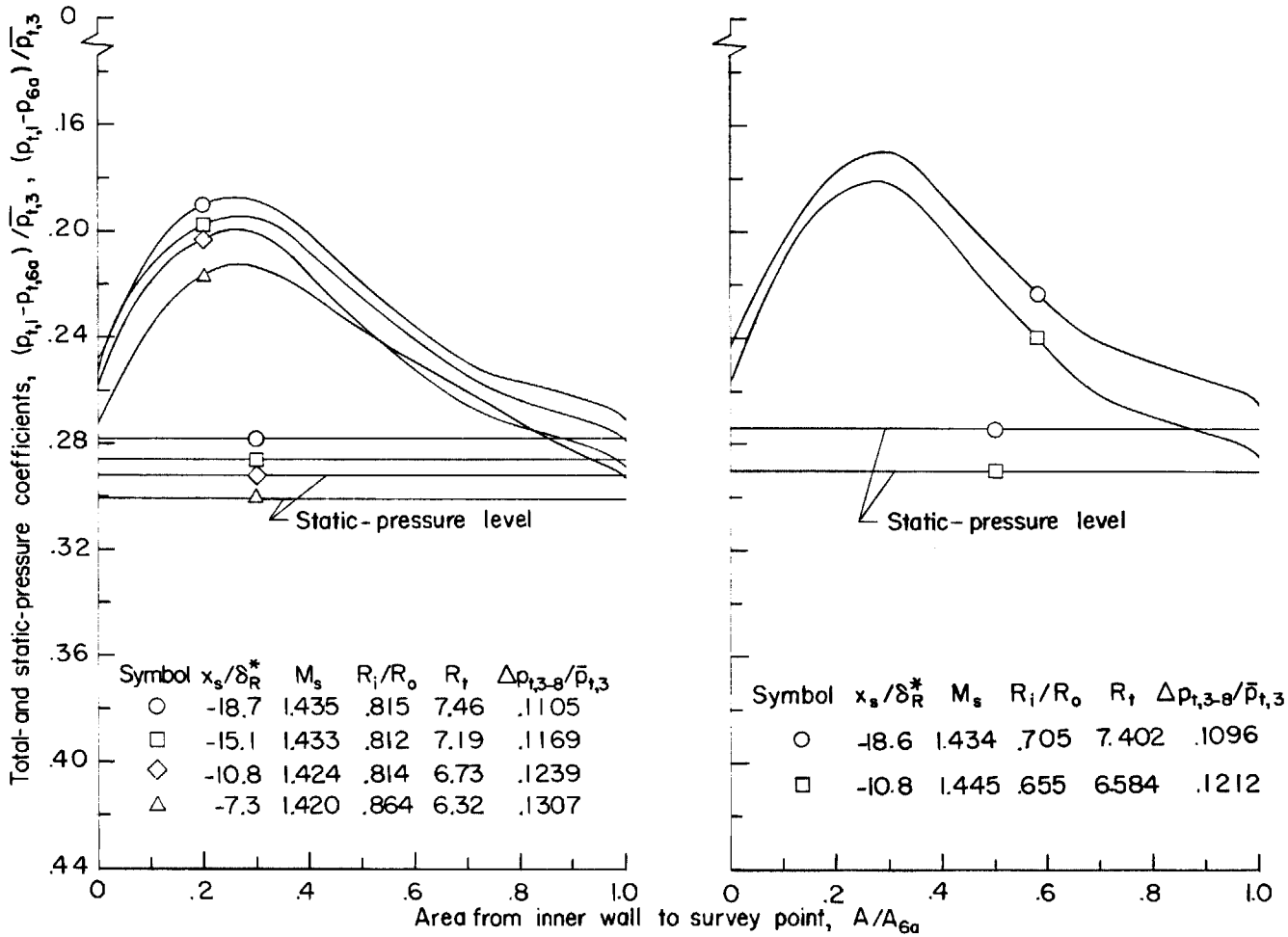

(a) Four suction rows.

(b) Six suction rows.

Figure 7.- Effect of shock position on total-pressure-loss and static-pressure-drop distributions. Symbols on curves do not represent test points, but are used merely to identify the curves.

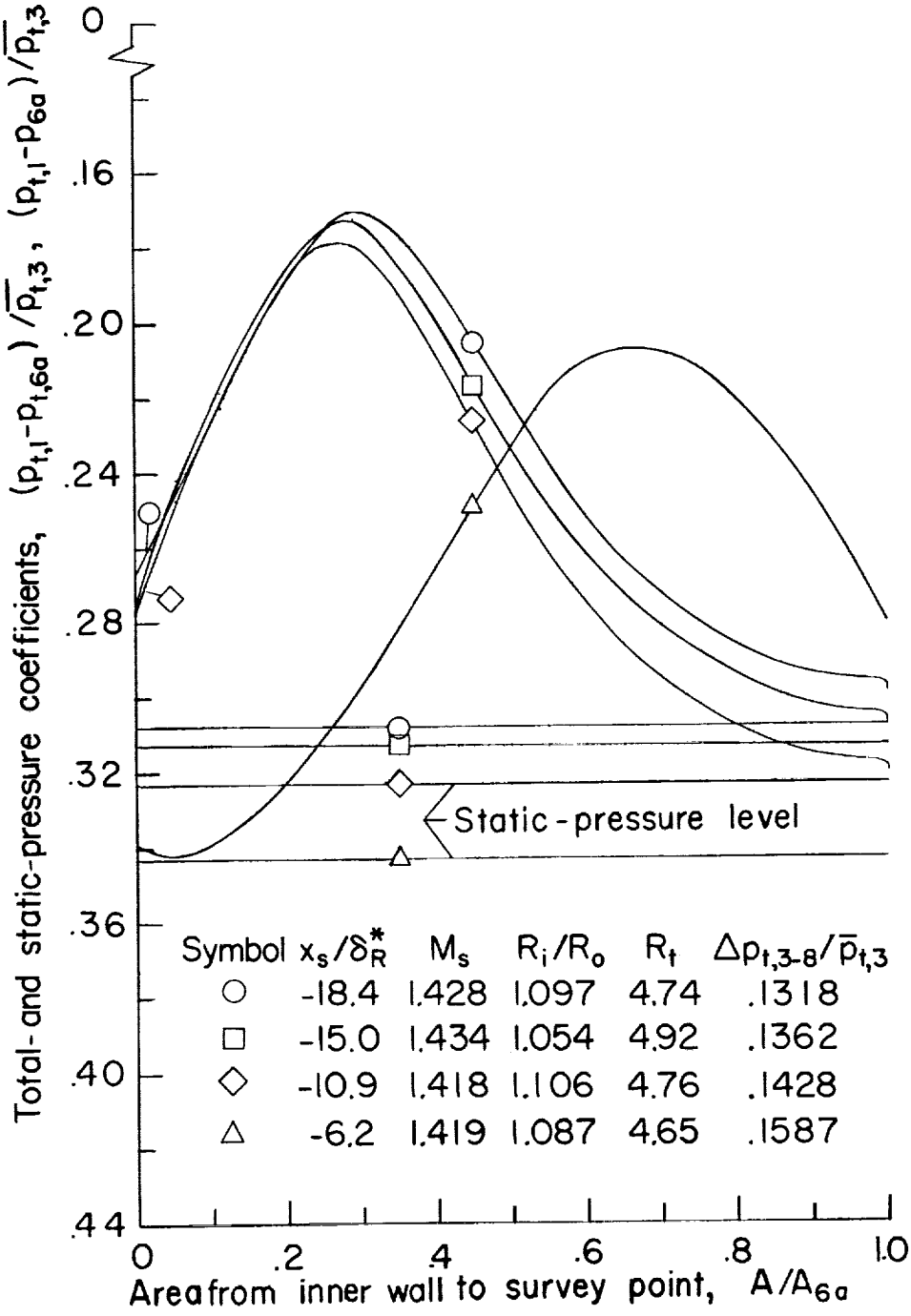

(c) Eight suction rows.

Figure 7.- Concluded.

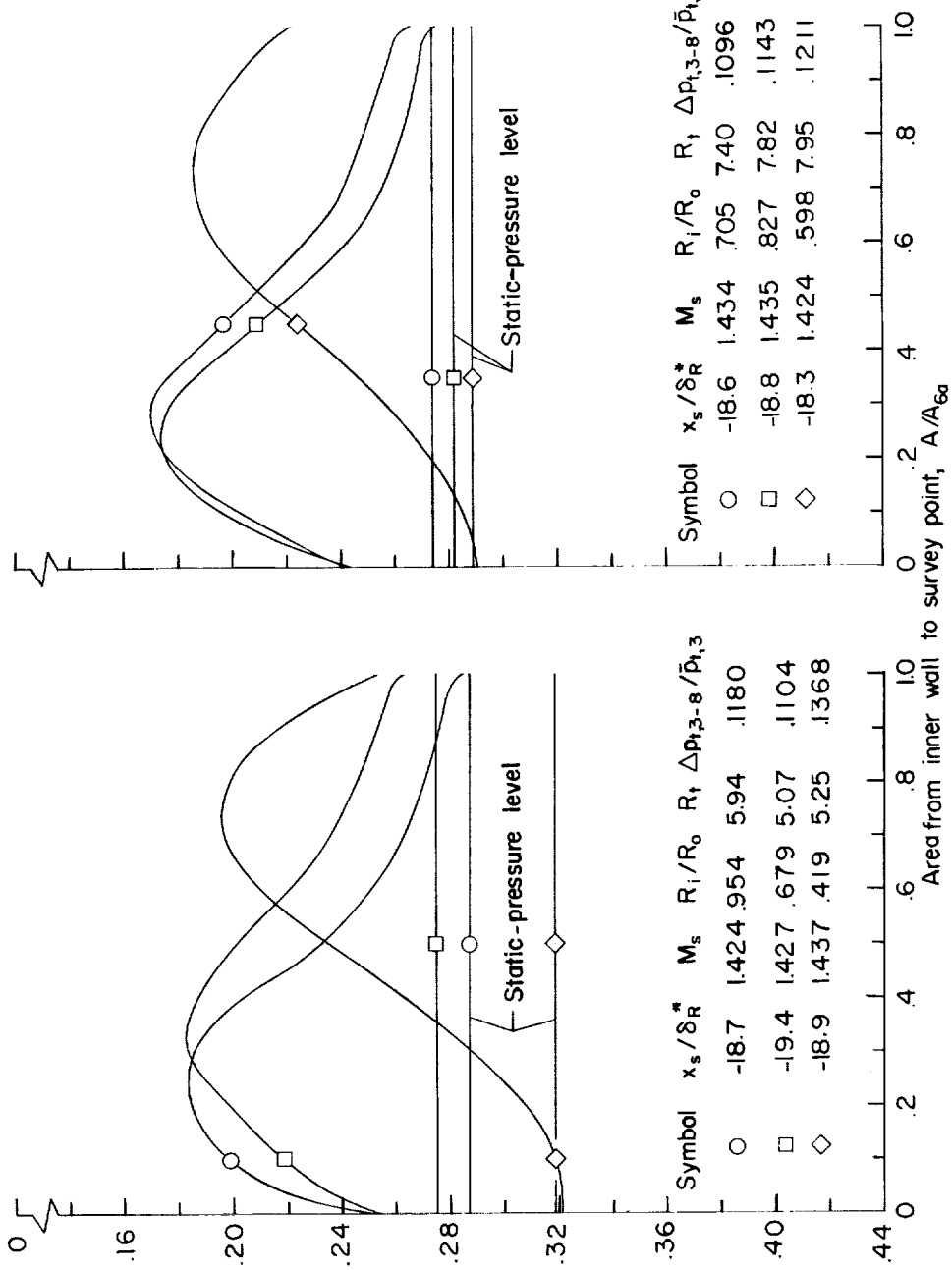

(a) Four suction rows.

(b) Six suction rows.

Figure 8.- Effect of inner-to-outer-wall suction-flow ratio on total-pressure-loss and static-pressure-drop distributions. Symbols on curves do not represent test points, but are used merely to identify the curves.

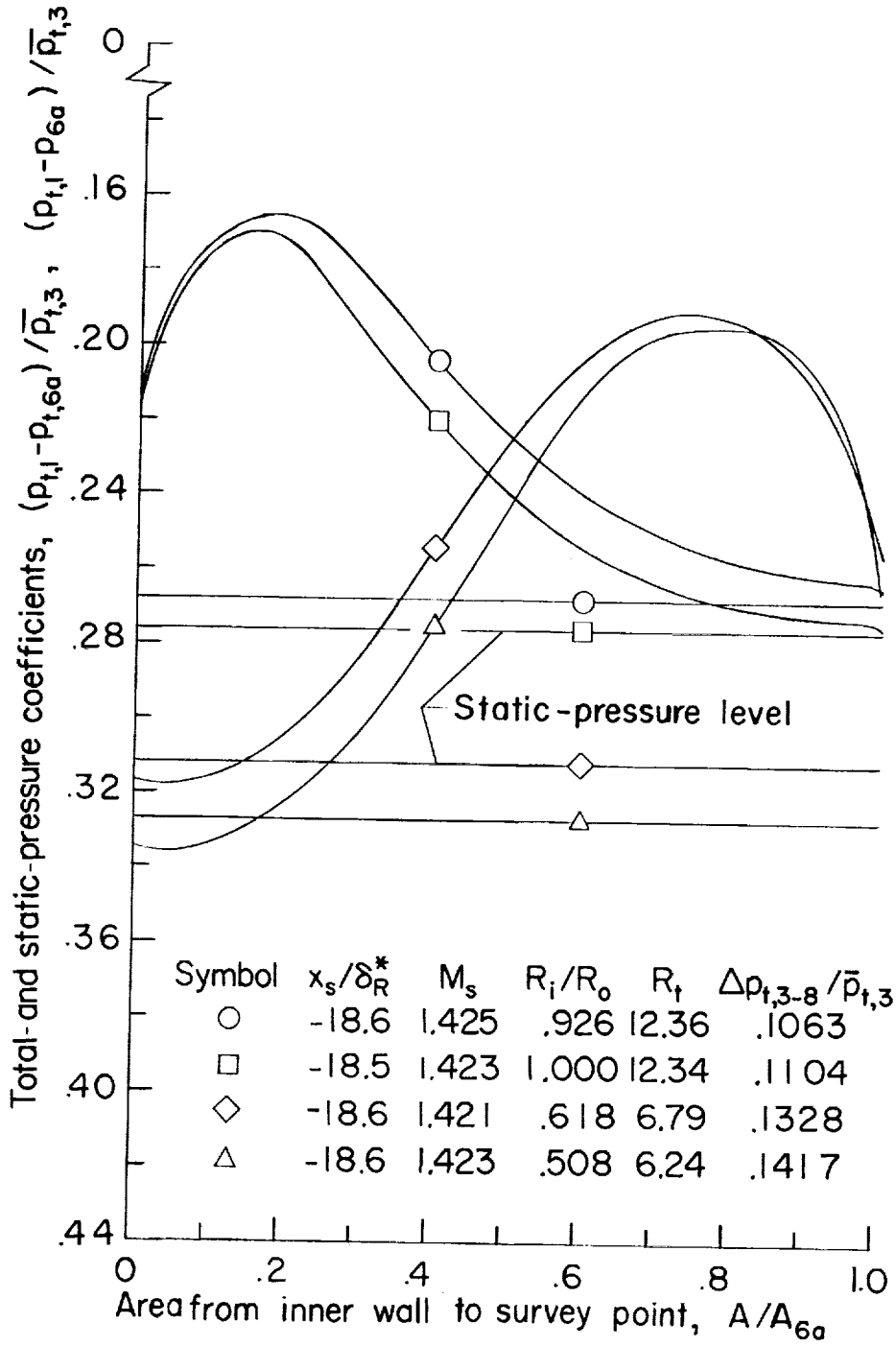

(c) Eight suction rows.

Figure 8.- Concluded.

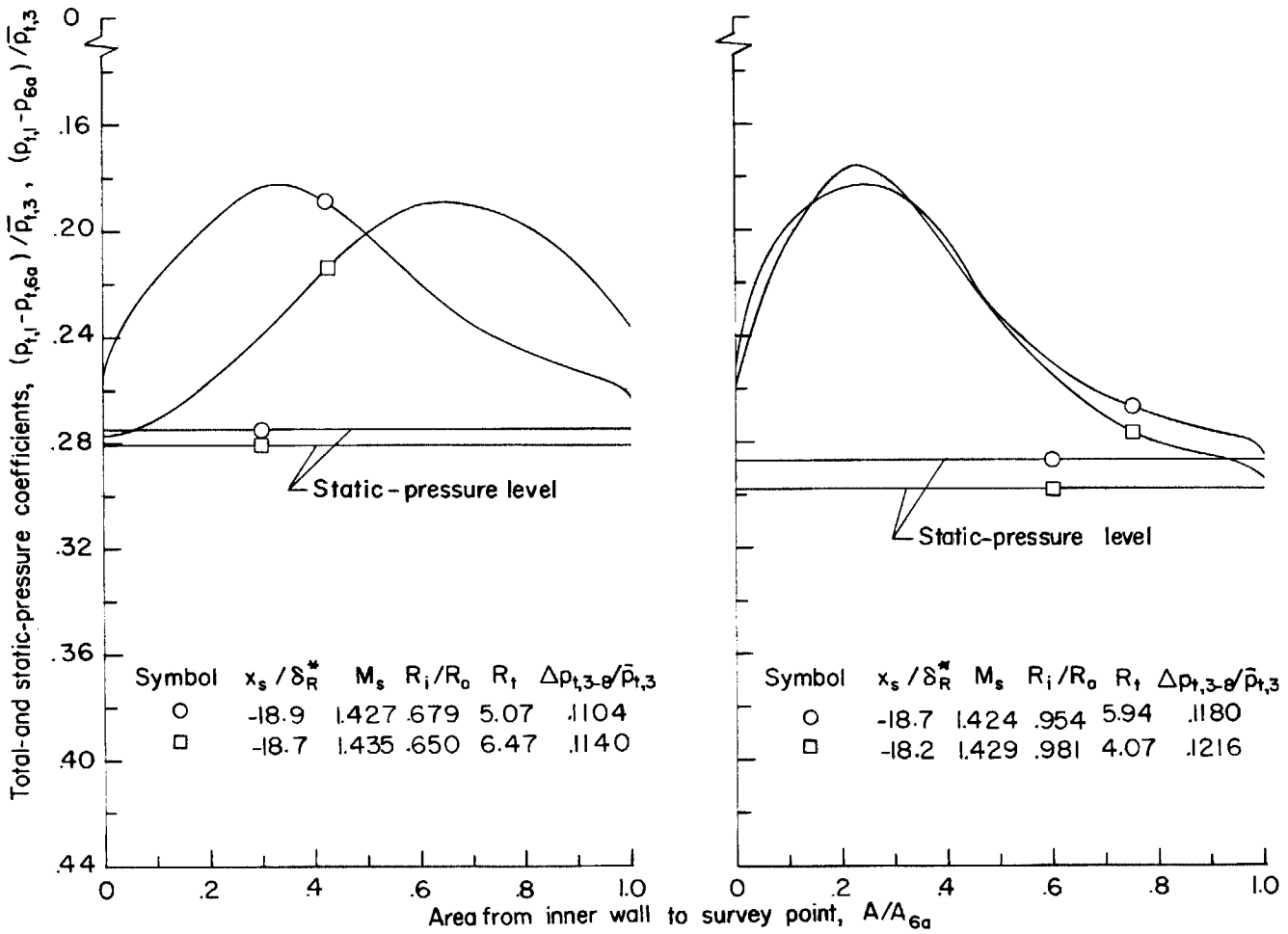

(a) Four suction rows.

Figure 9.- Effect of total suction flow on total-pressure-loss and static-pressure-drop distributions. Symbols on curves do not represent test points, but are used merely to identify the curves.

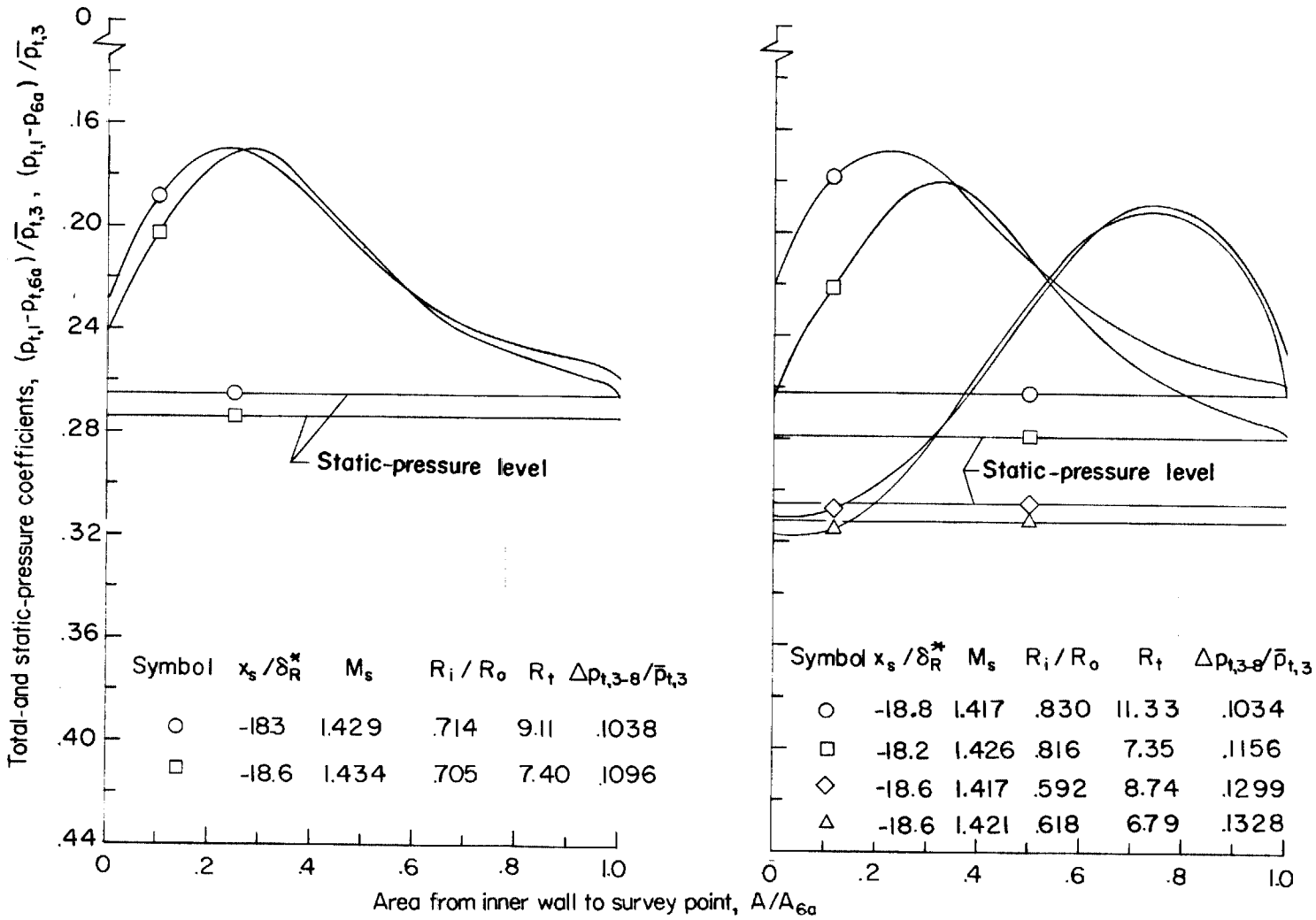

(b) Six suction rows.

(c) Eight suction rows.

Figure 9.- Concluded.

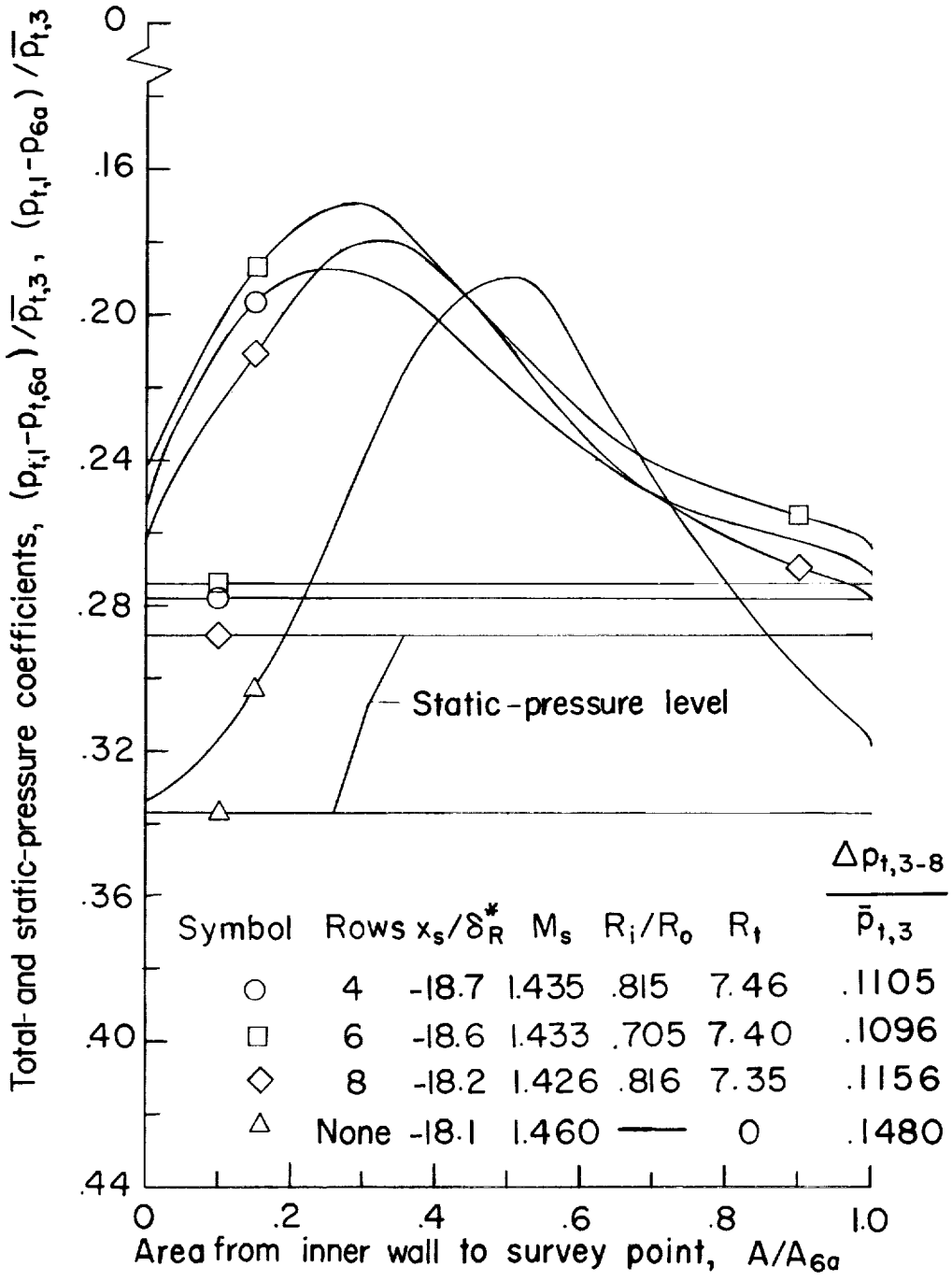

Figure 10.- Effect of hole pattern on total-pressure-loss and static-pressure-drop distributions. Symbols on curves do not represent test points, but are used merely to identify the curves.

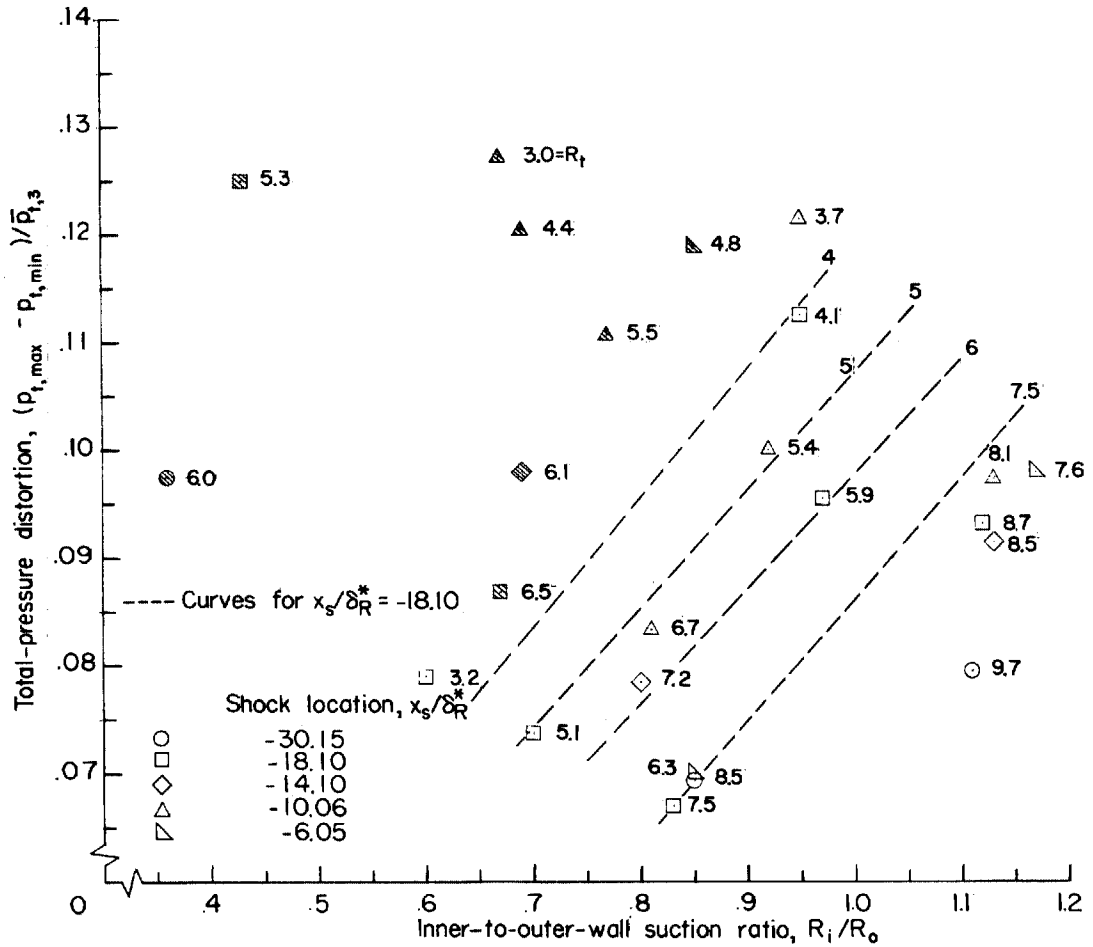

(a) Four suction rows.

Figure 11.- Total-pressure distortion at station 6a for several shock locations. Shaded symbols denote separated flow; numerals indicate the total suction R_t.

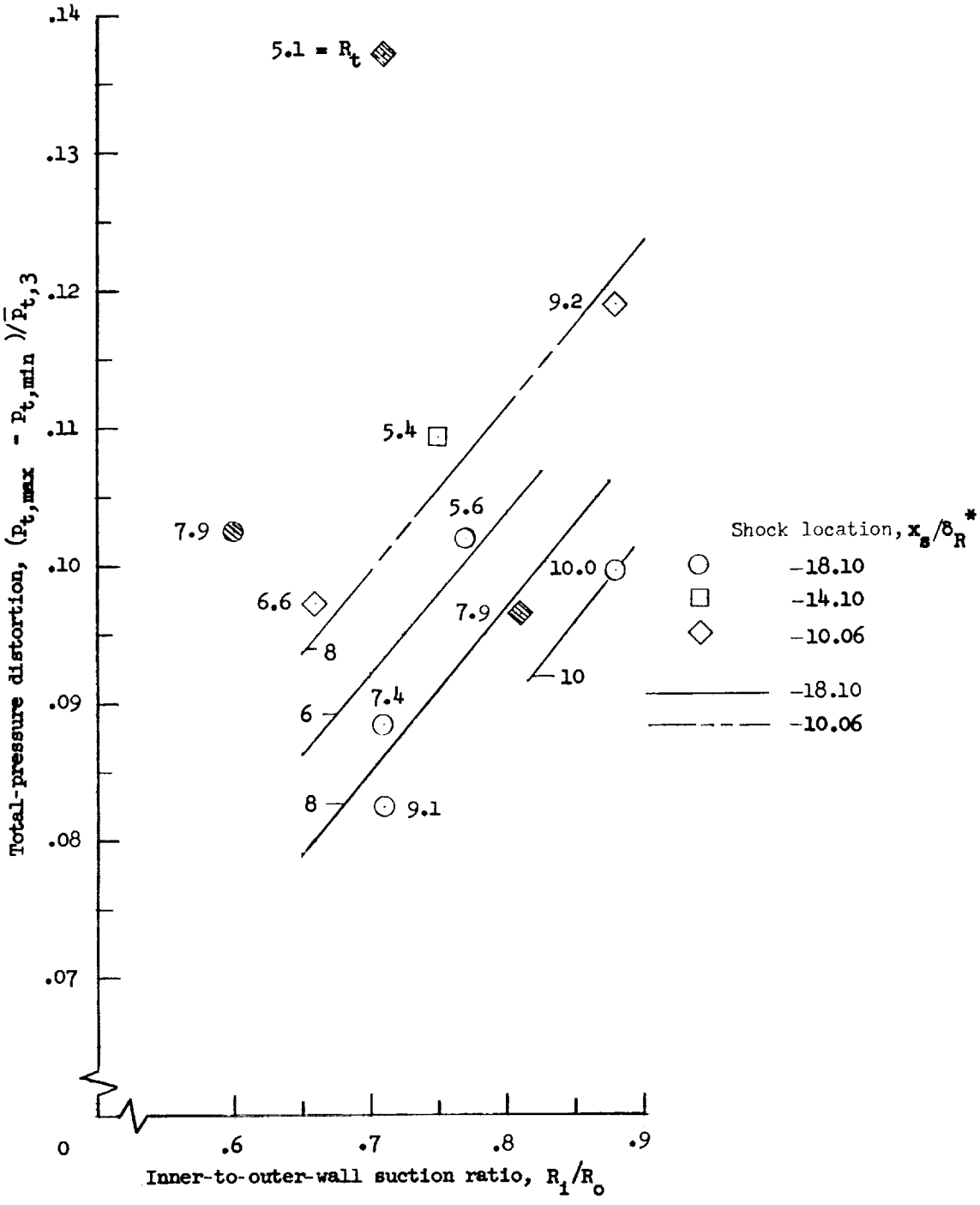

(b) Six suction rows.

Figure 11.- Continued.

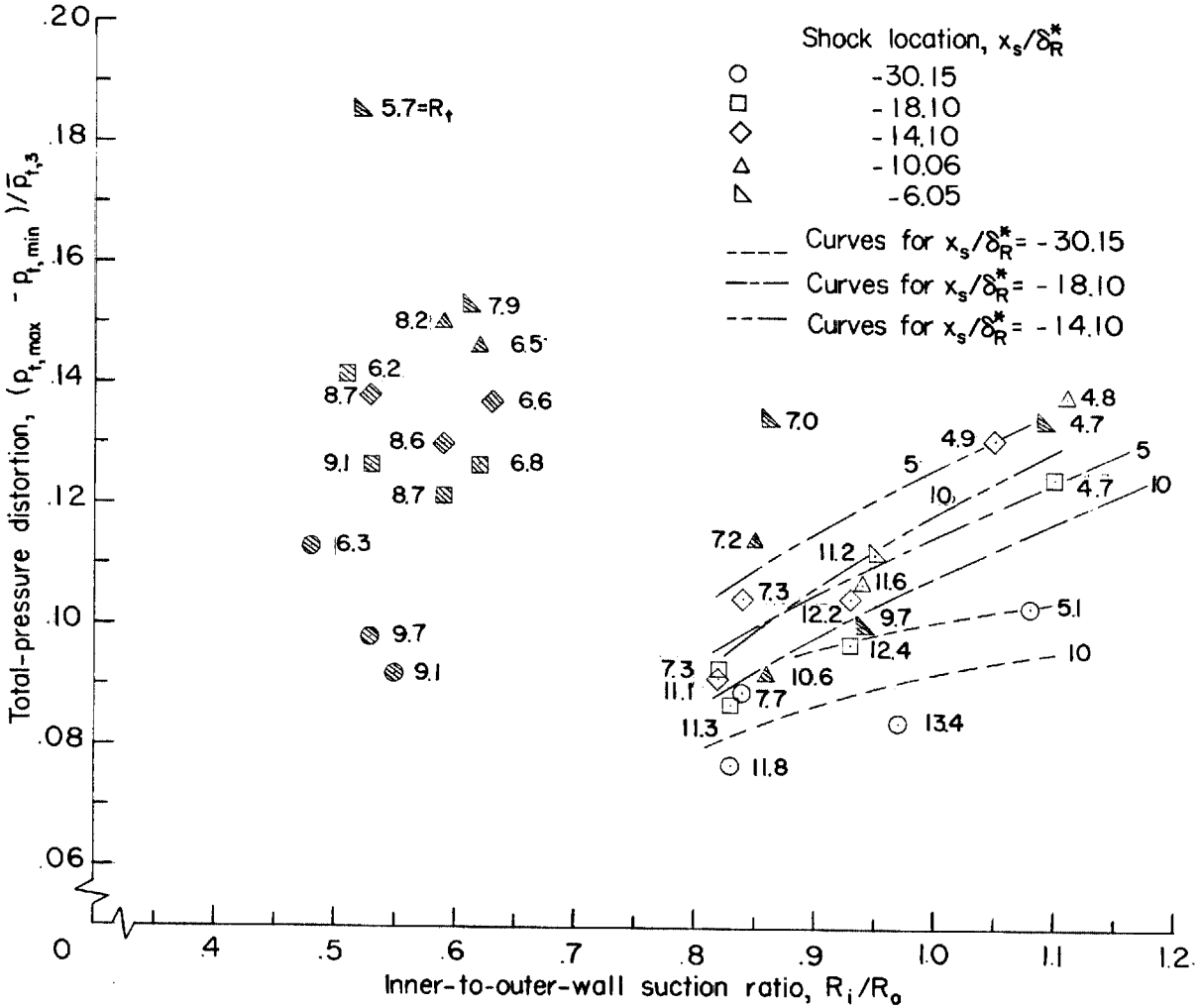

(c) Eight suction rows.

Figure 11.- Concluded.

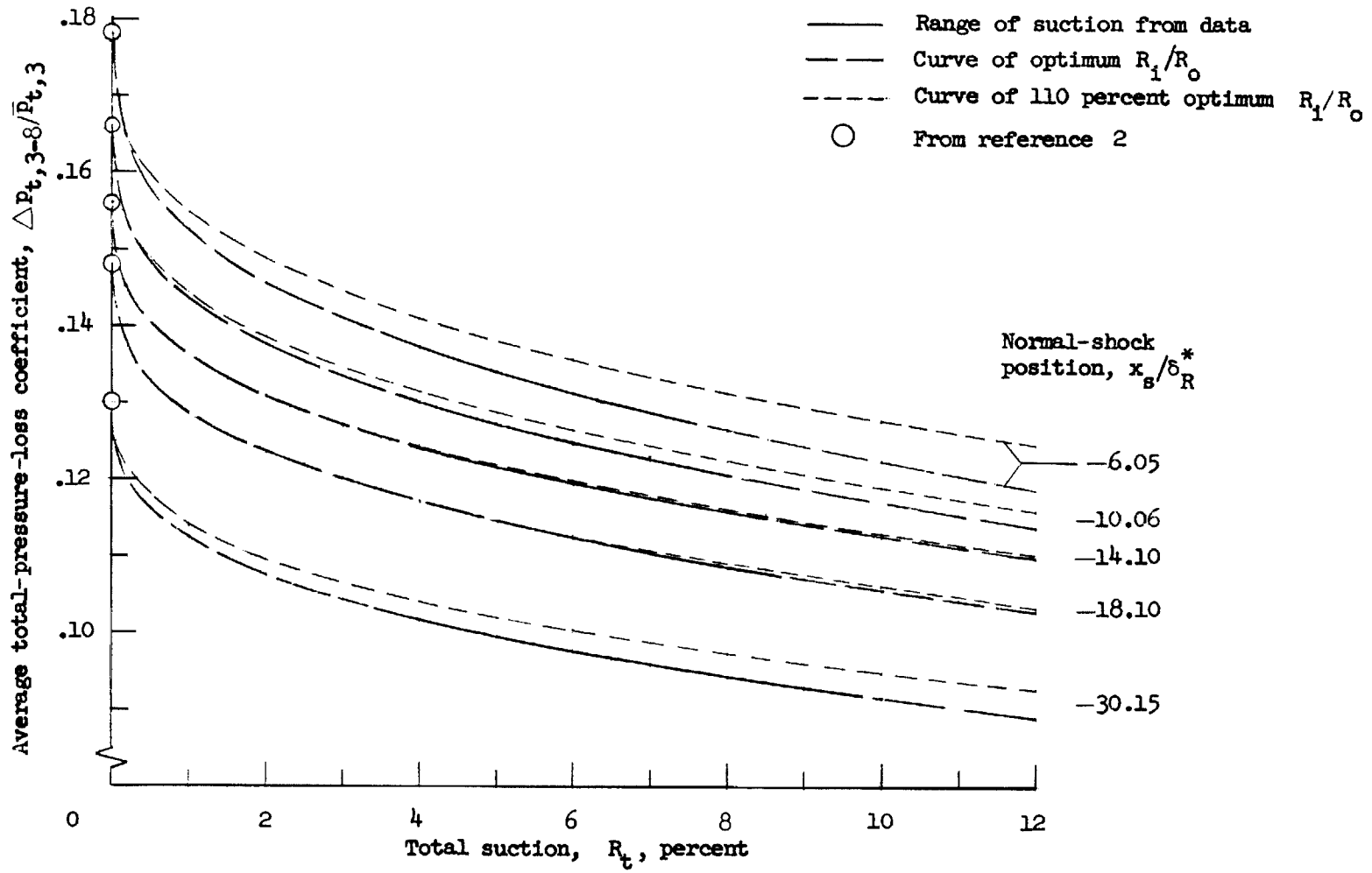

(a) Four suction rows.

Figure 12.- Average total-pressure-loss coefficient for a range of suction flows.

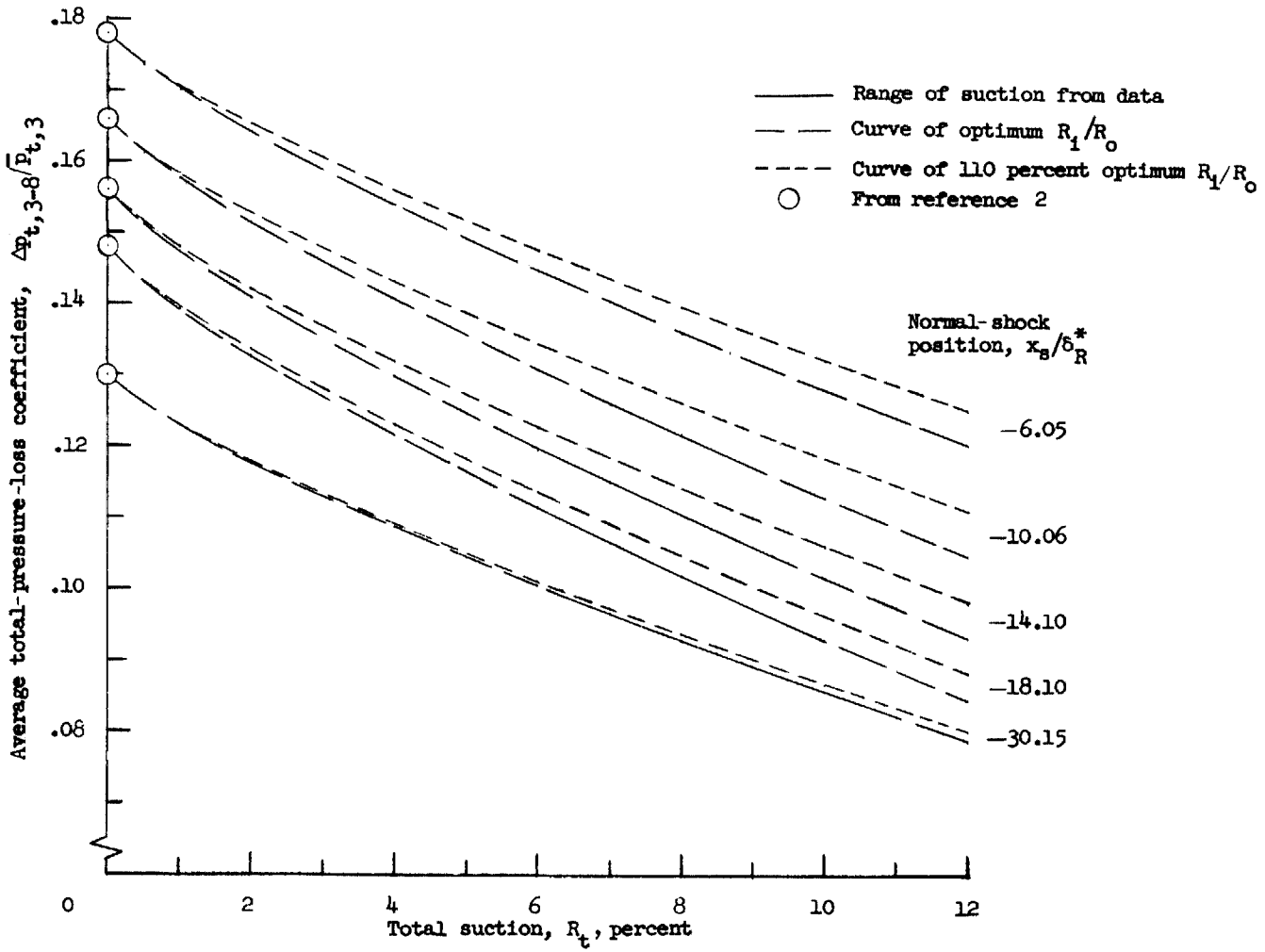

(b) Six suction rows.

Figure 12.- Continued.

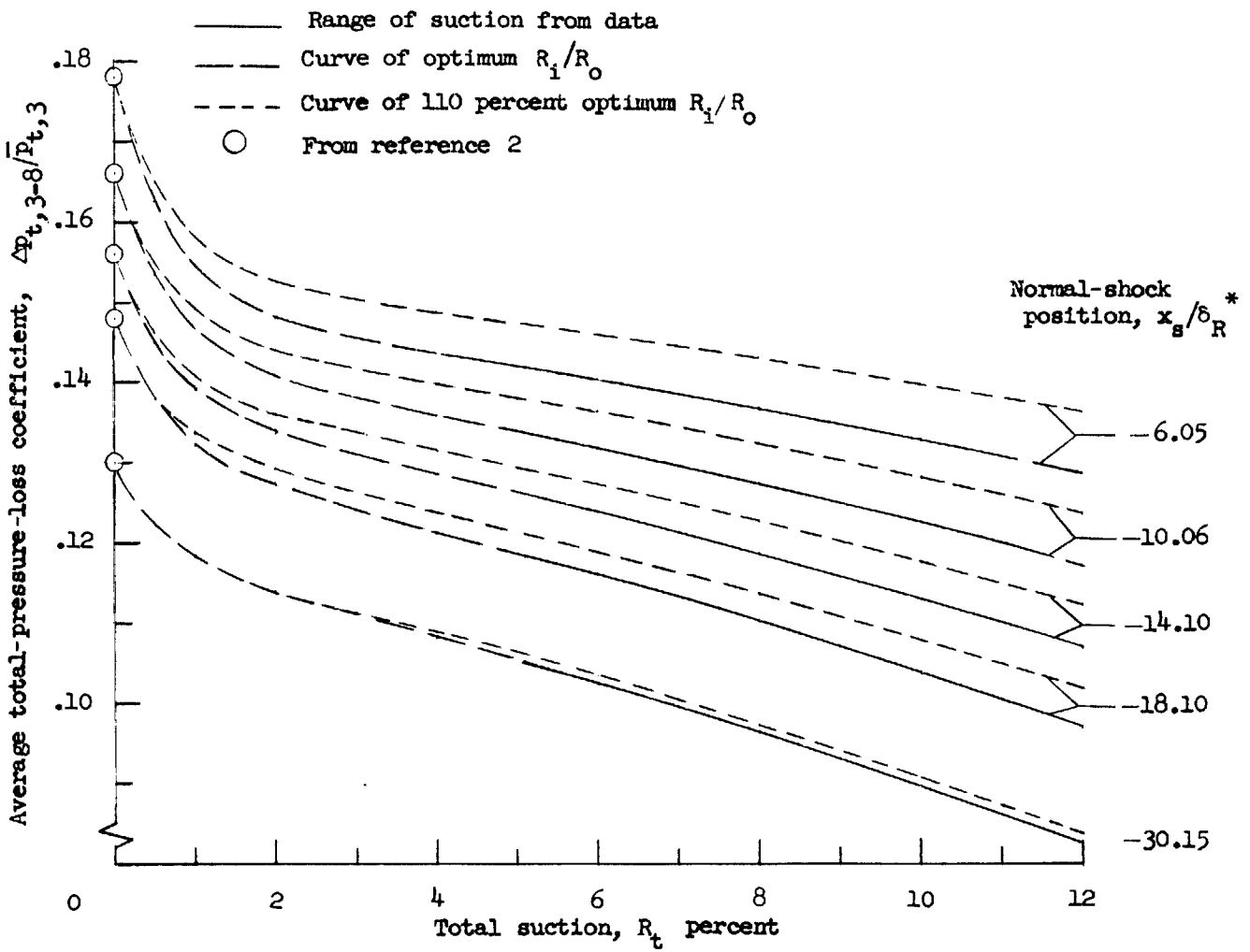

(c) Eight suction rows.

Figure 12.- Concluded.

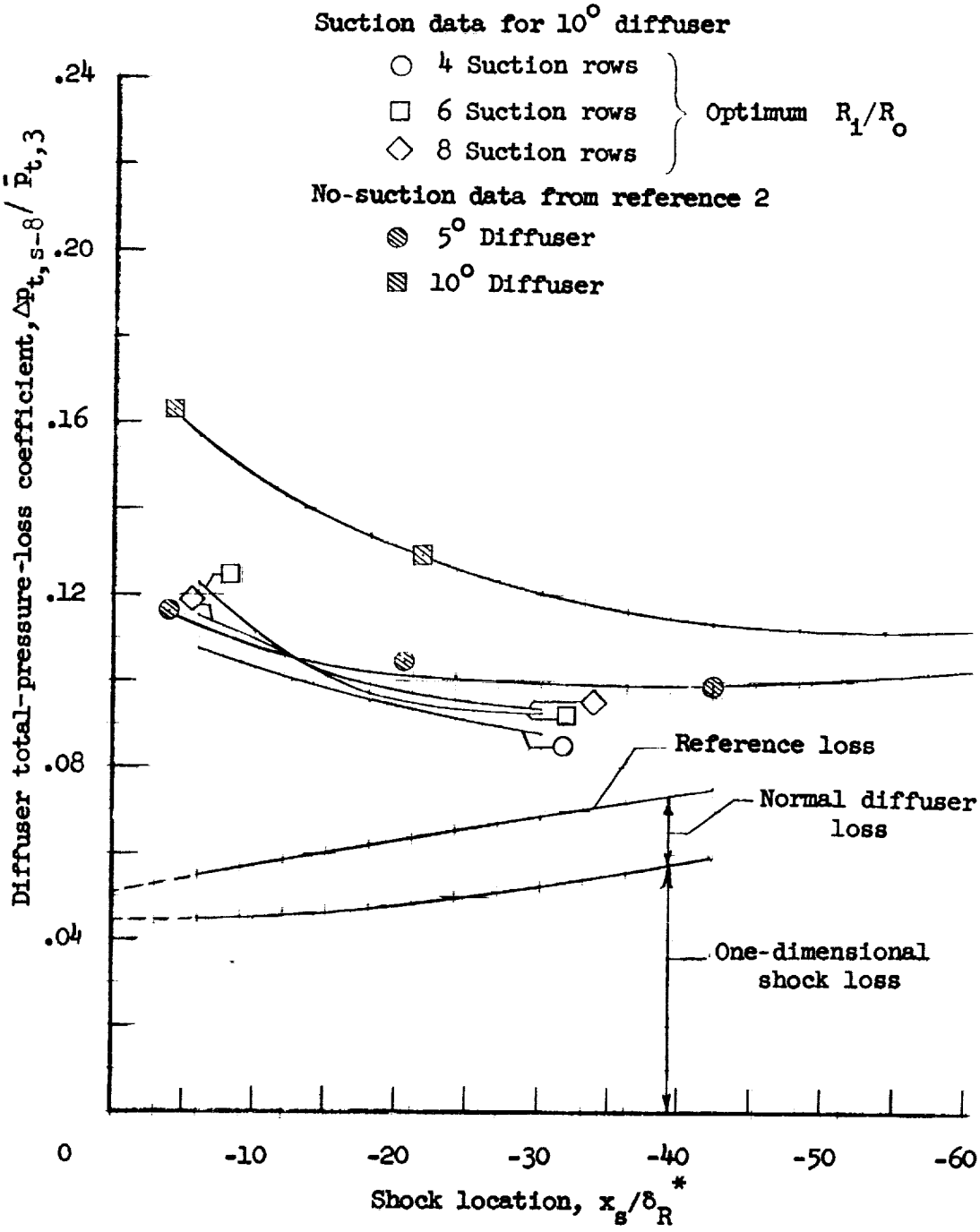

(a) R_t = 5 percent.

Figure 13.- Minimum diffuser total-pressure loss at various shock locations.

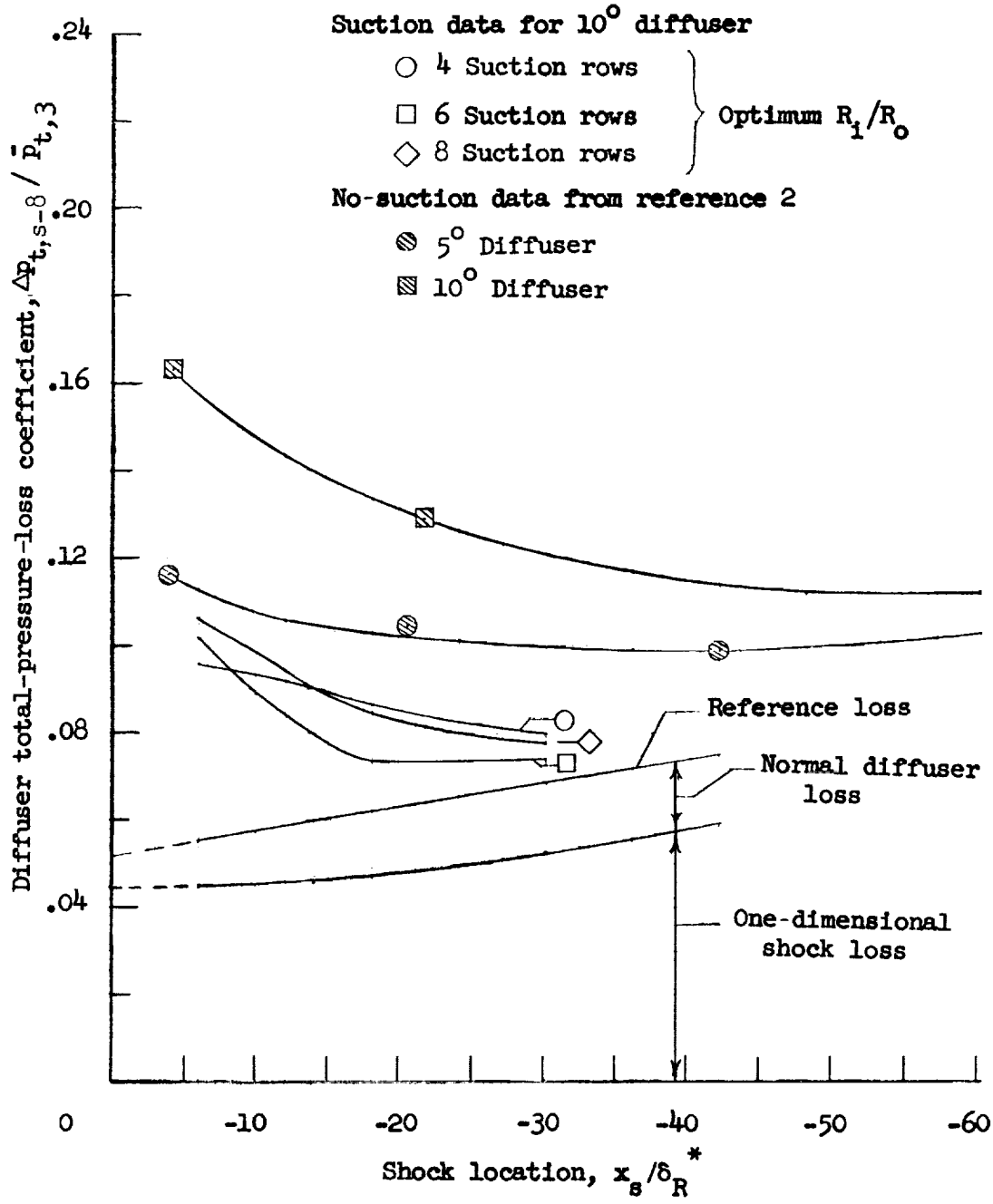

(b) R_t = 10 percent.

Figure 13.- Concluded.

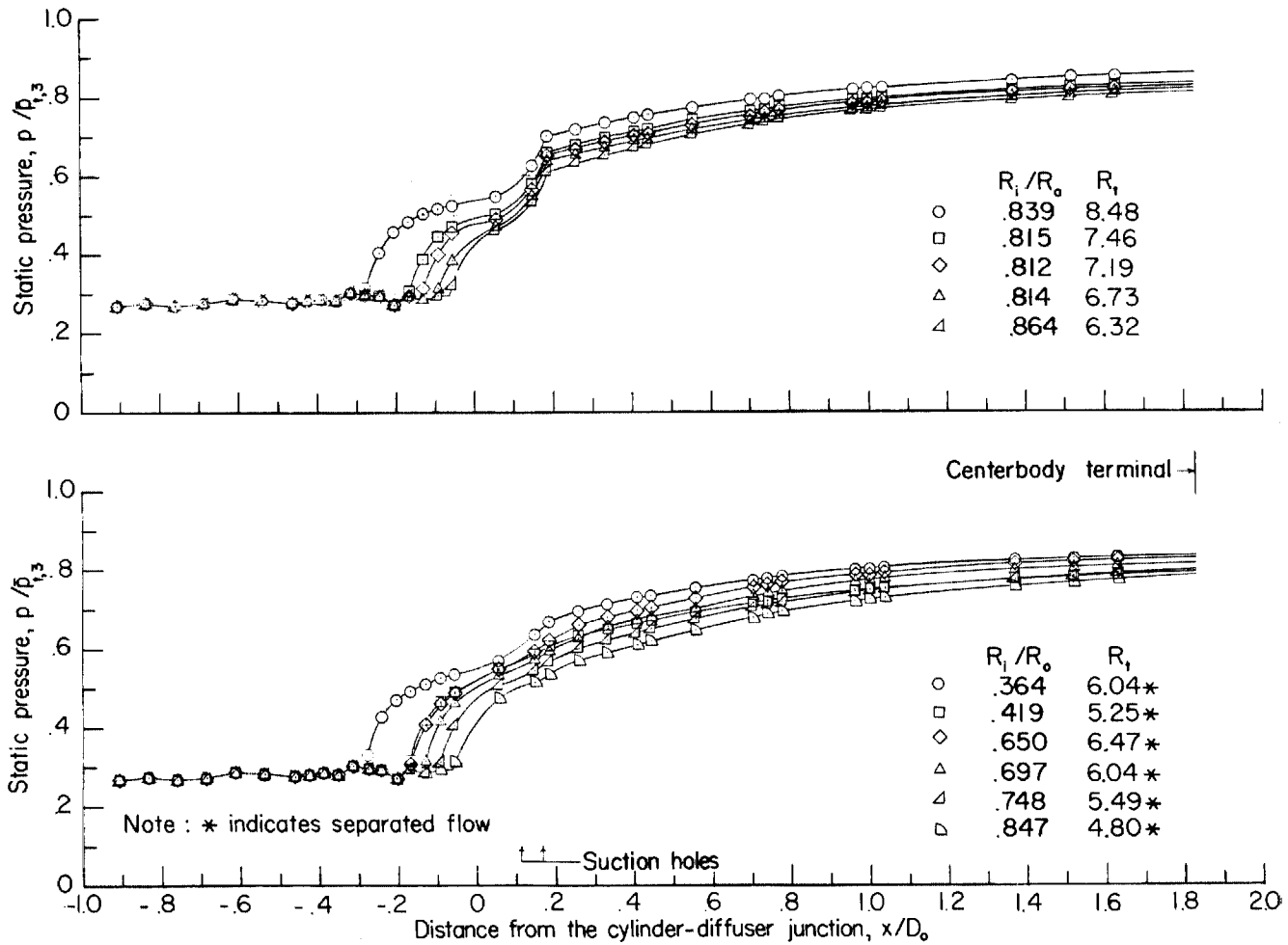

(a) Four suction rows.

Figure 14.- Inner-wall longitudinal static-pressure distributions for several shock locations.

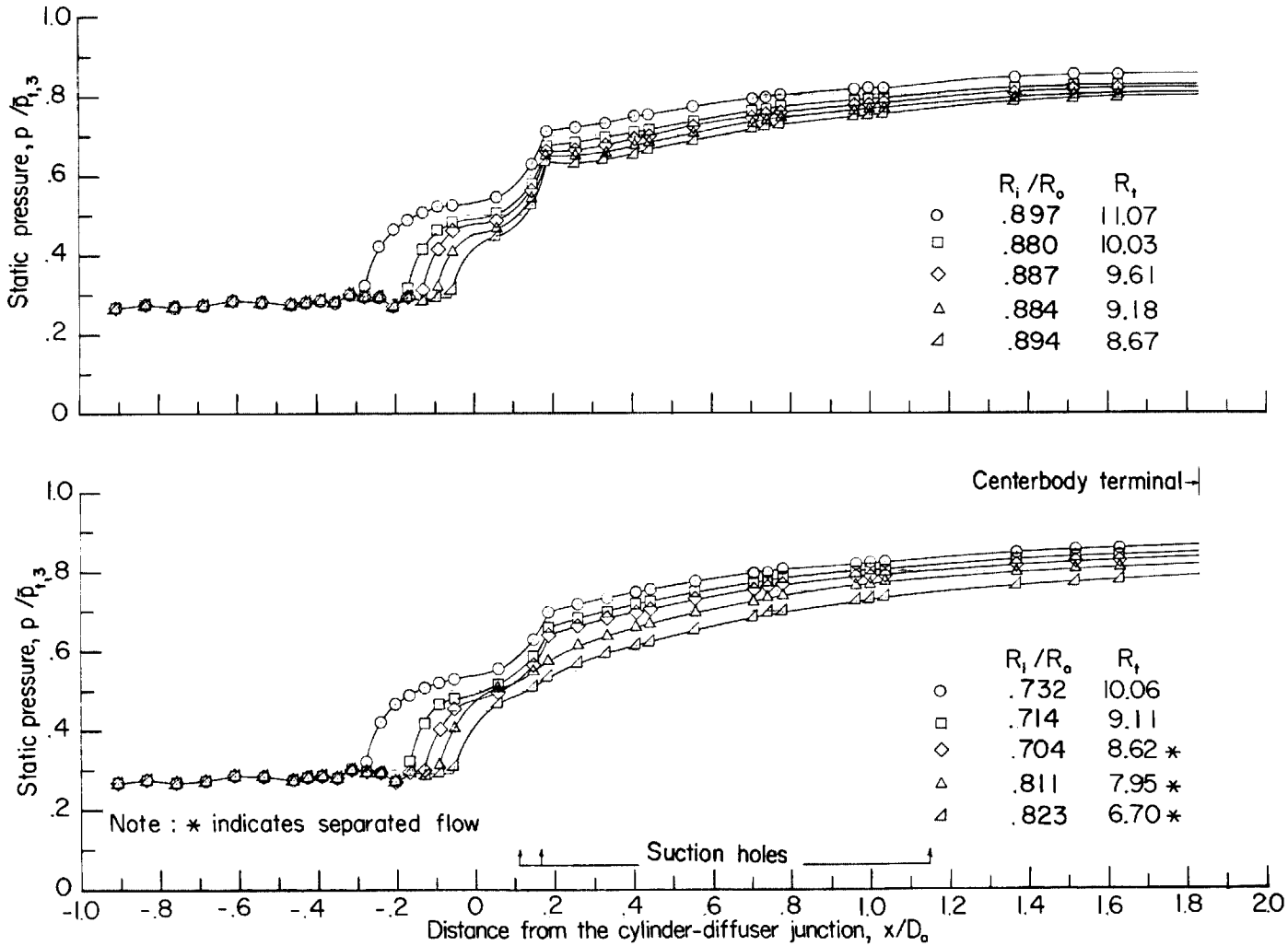

(b) Six suction rows.

Figure 14.- Continued.

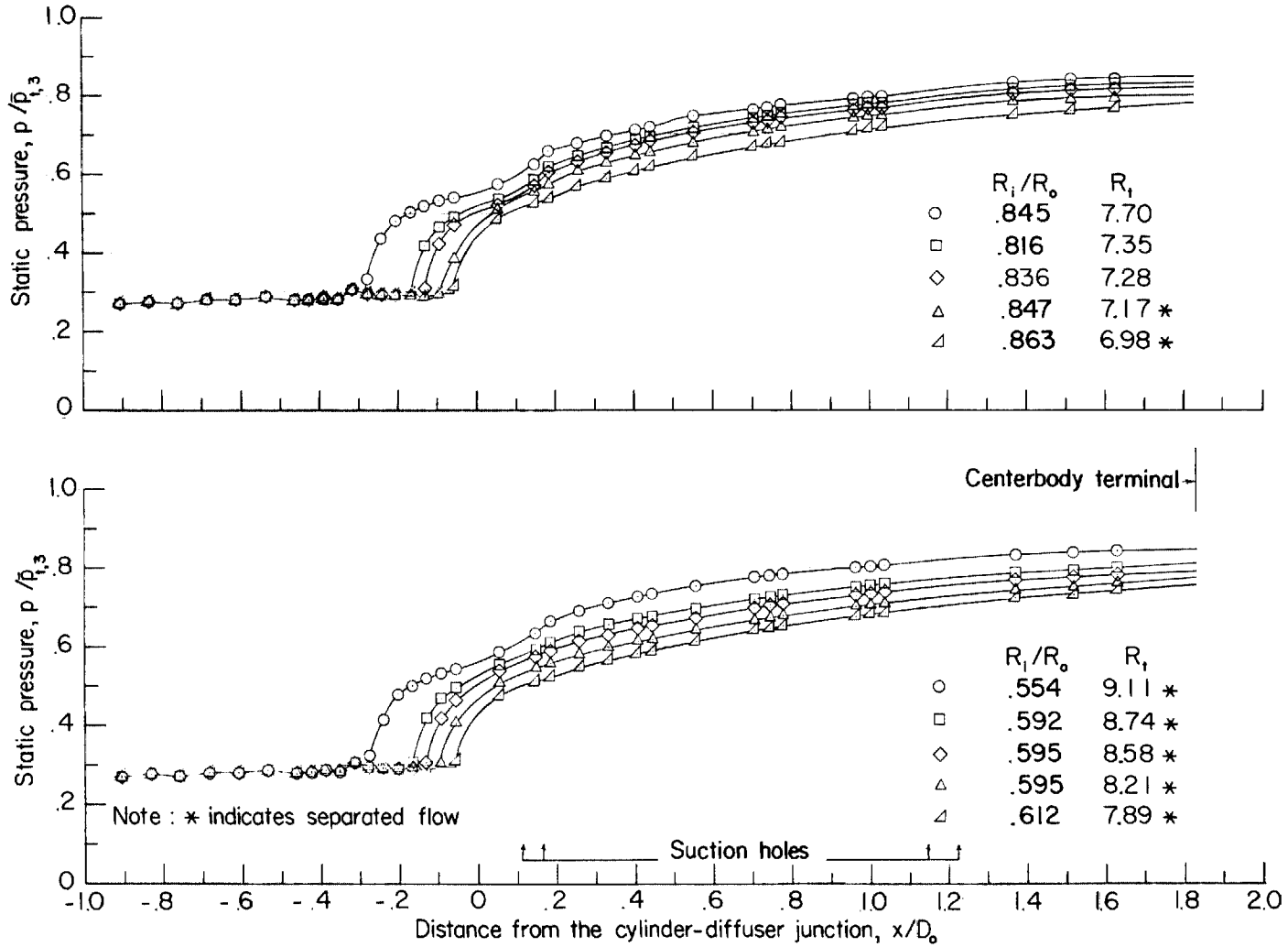

(c) Eight suction rows.

Figure 14.- Concluded.

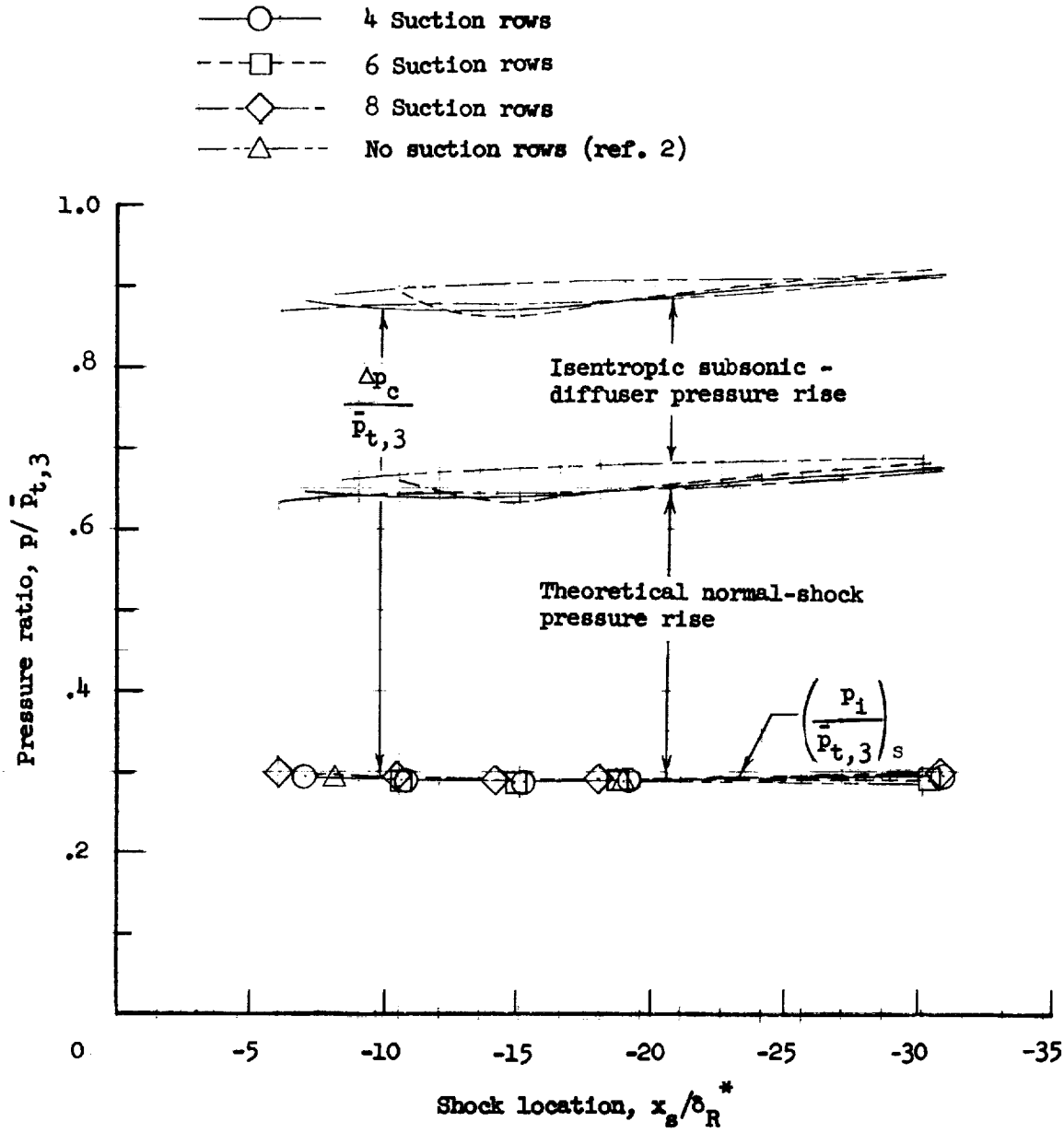

Figure 15.- Theoretical diffuser static-pressure rise due to normal shock and isentropic diffusion; total suction flow of approximately 7 percent.

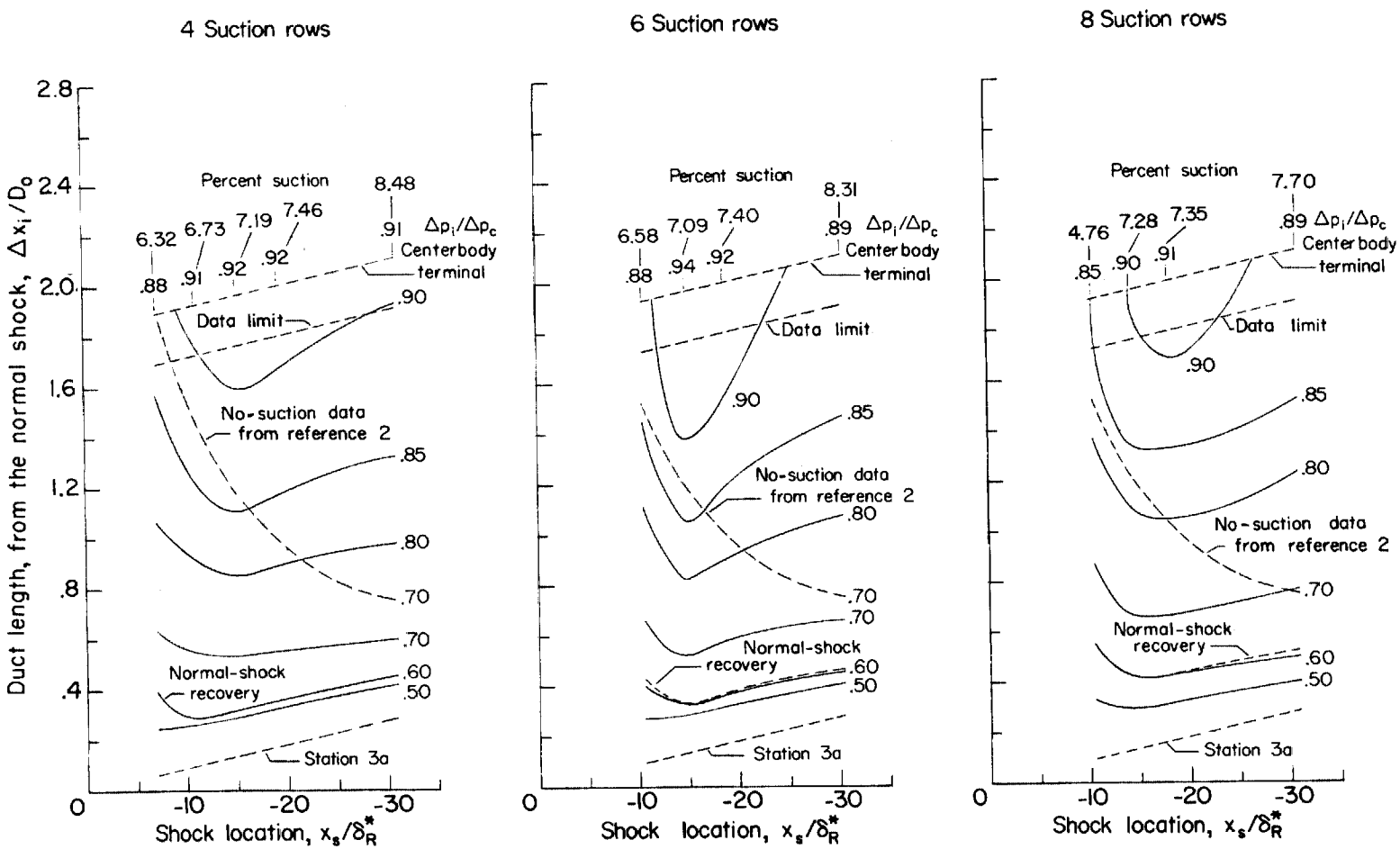

Figure 16.- Duct lengths required to recover the theoretical static-pressure rise on the diffuser inner wall for approximately 7-percent total suction.

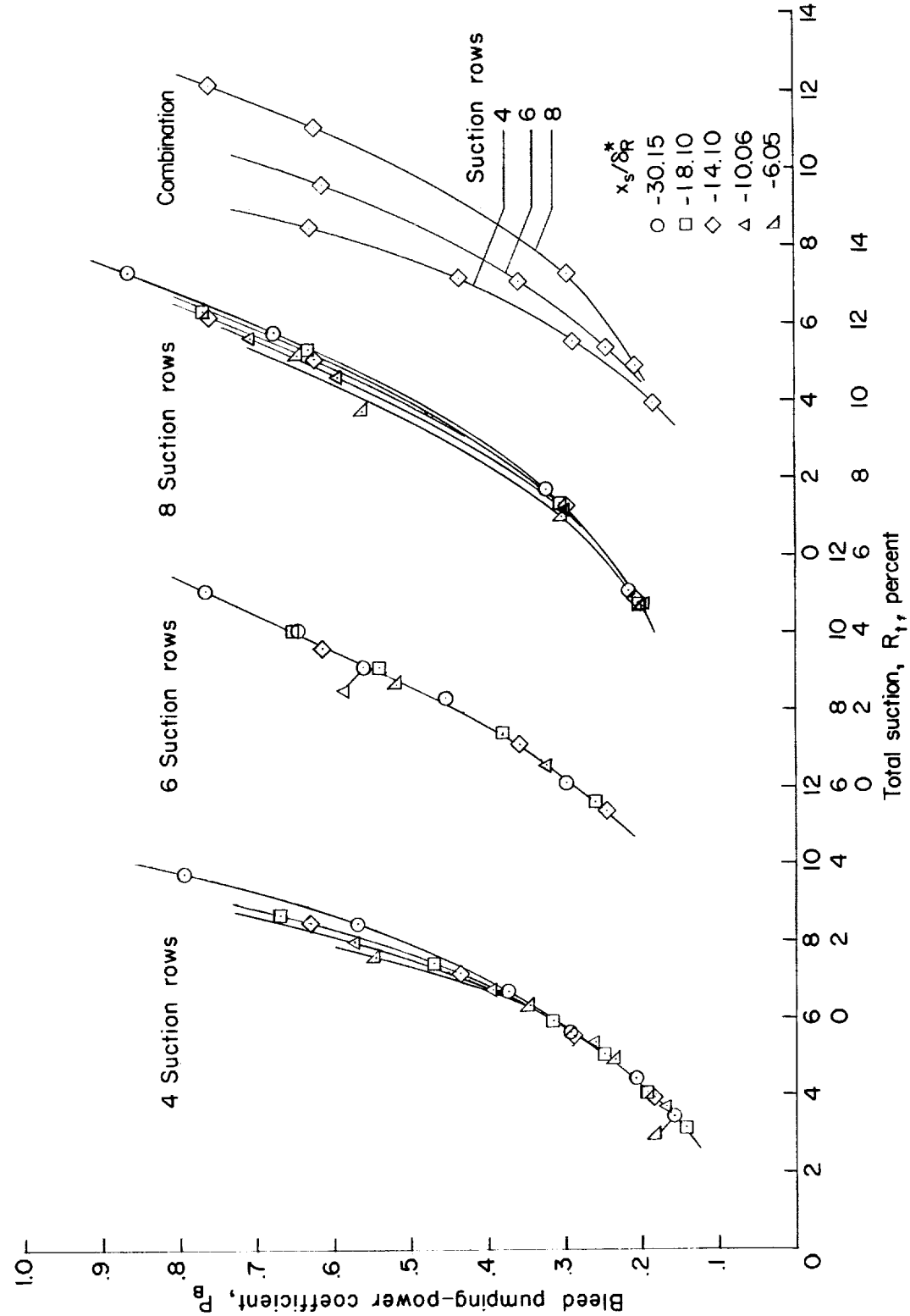

Figure 17.- Bleed pumping-power coefficient for various amounts of suction. All points are for attached flow.

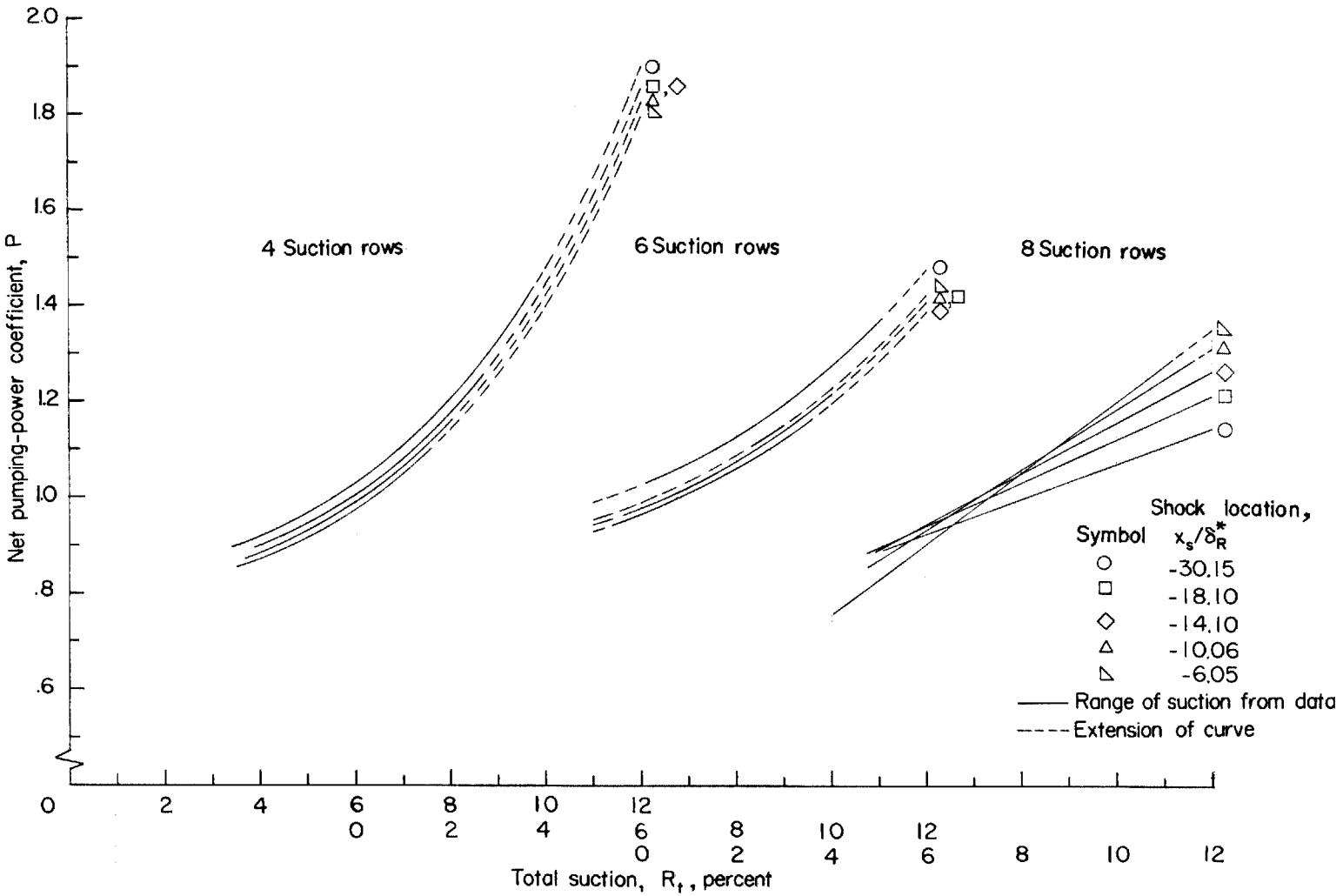

Figure 18.- Net pumping-power coefficient for various amounts of suction at optimum R_i/R_o. Symbols on curves do not represent test points, but are used merely to identify the curves.

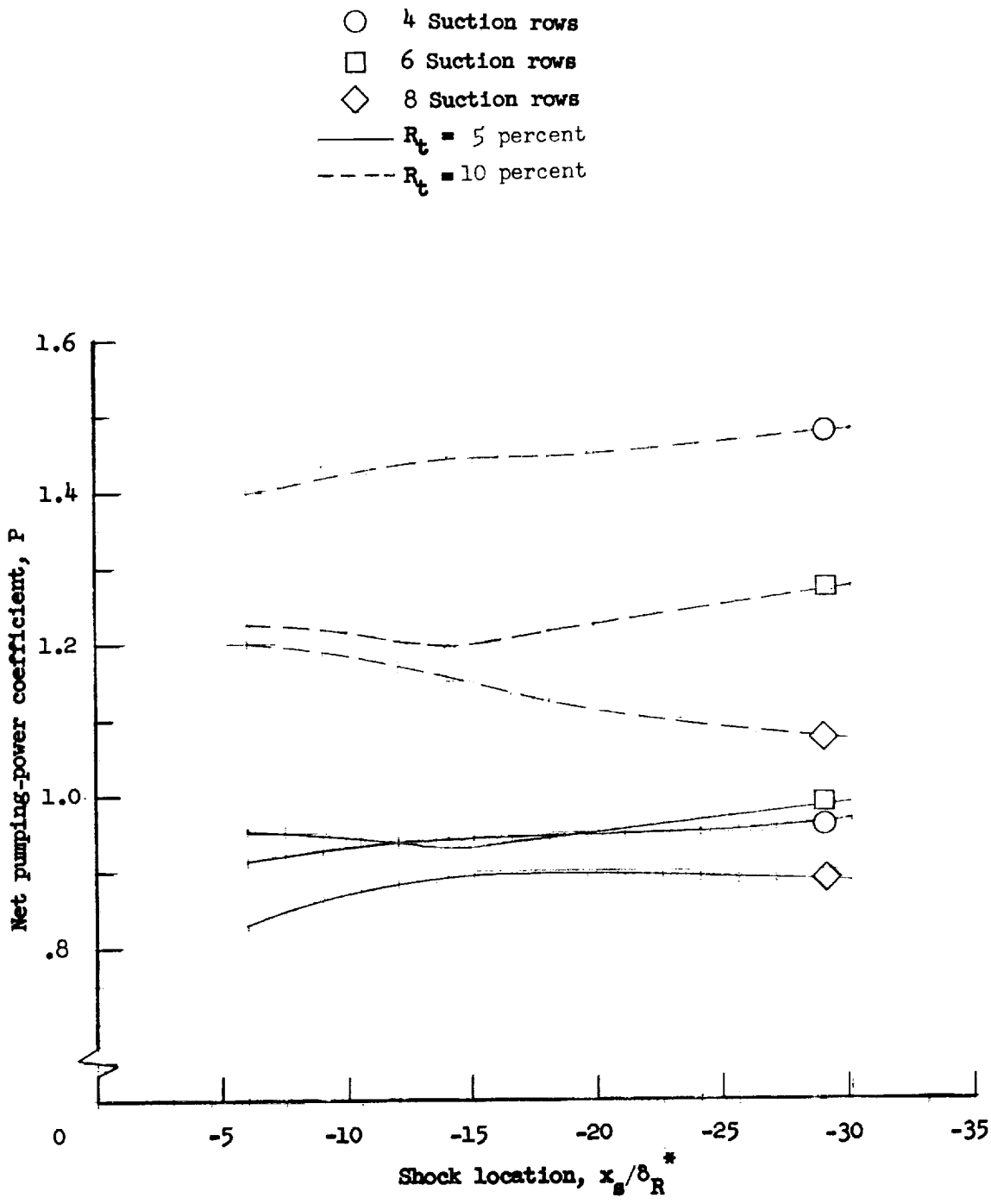

Figure 19.- Net pumping-power coefficient for several shock locations; optimum R_i/R_o. Symbols on curves do not represent test points, but are used merely to identify the curves.

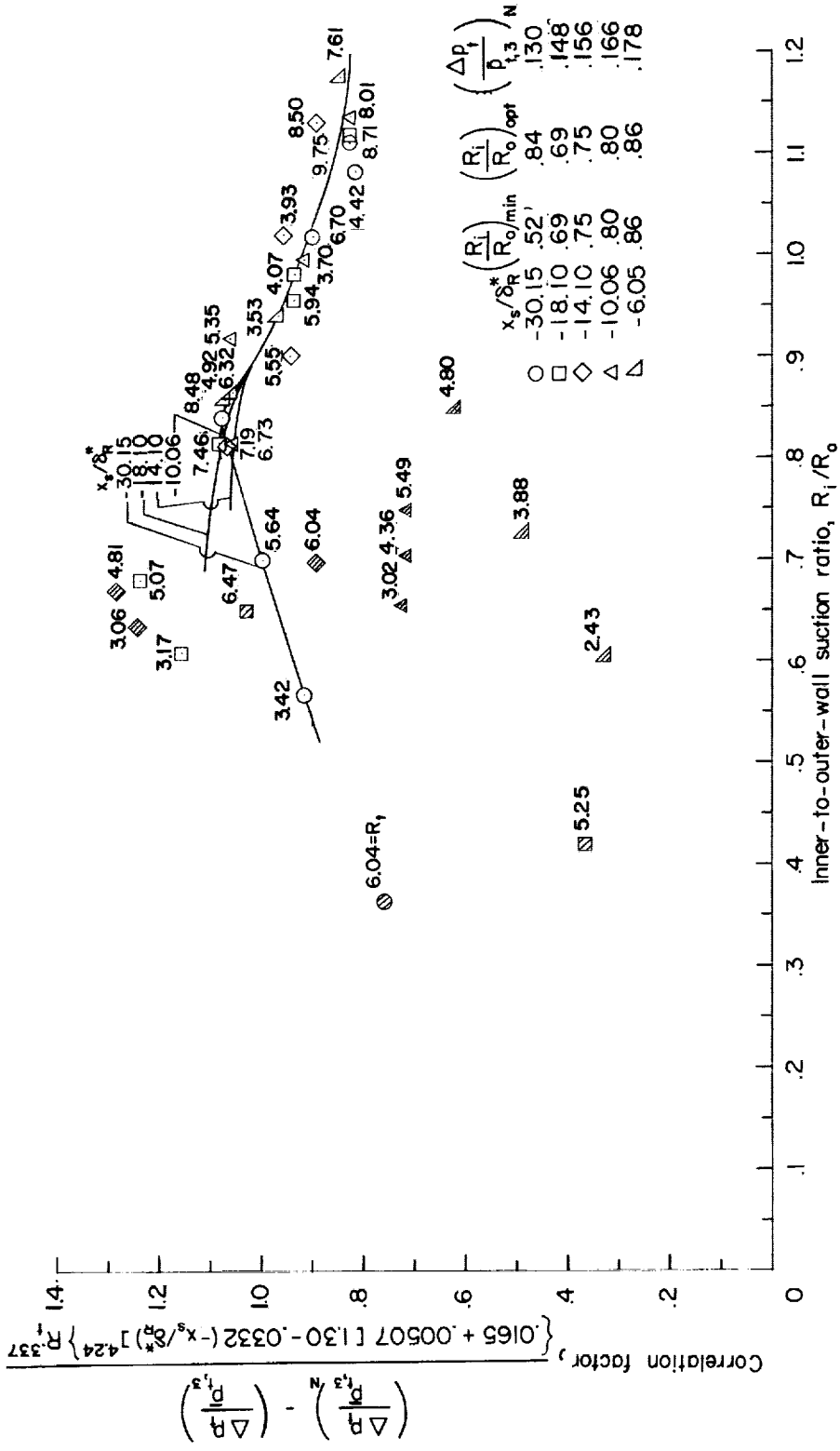

(a) Four suction rows.

Figure 20.- Average total-pressure-loss correlation factor. Shaded symbols denote separated flow; numerals indicate values of R_t.

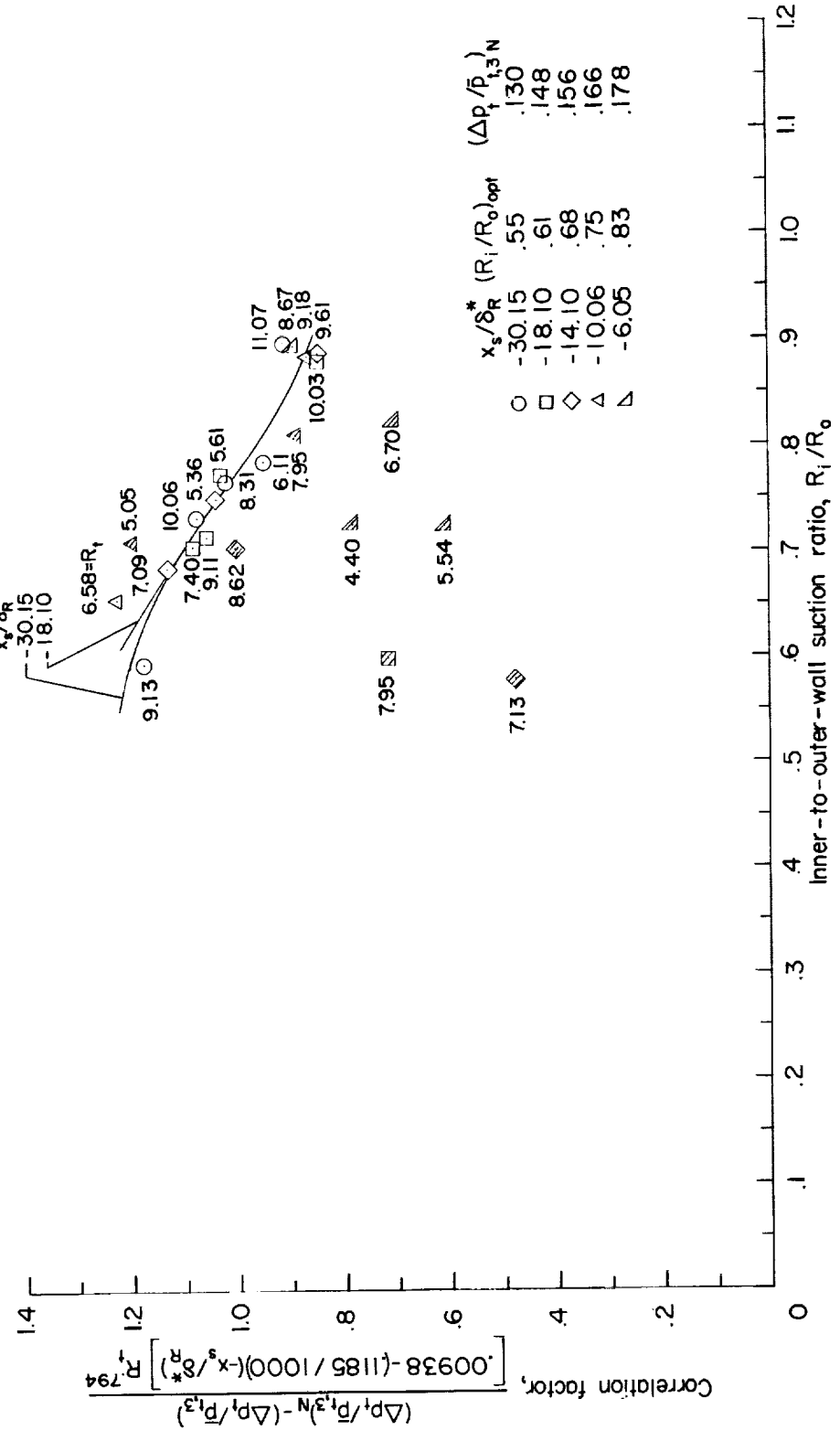

(b) Six suction rows.

Figure 20.- Continued.

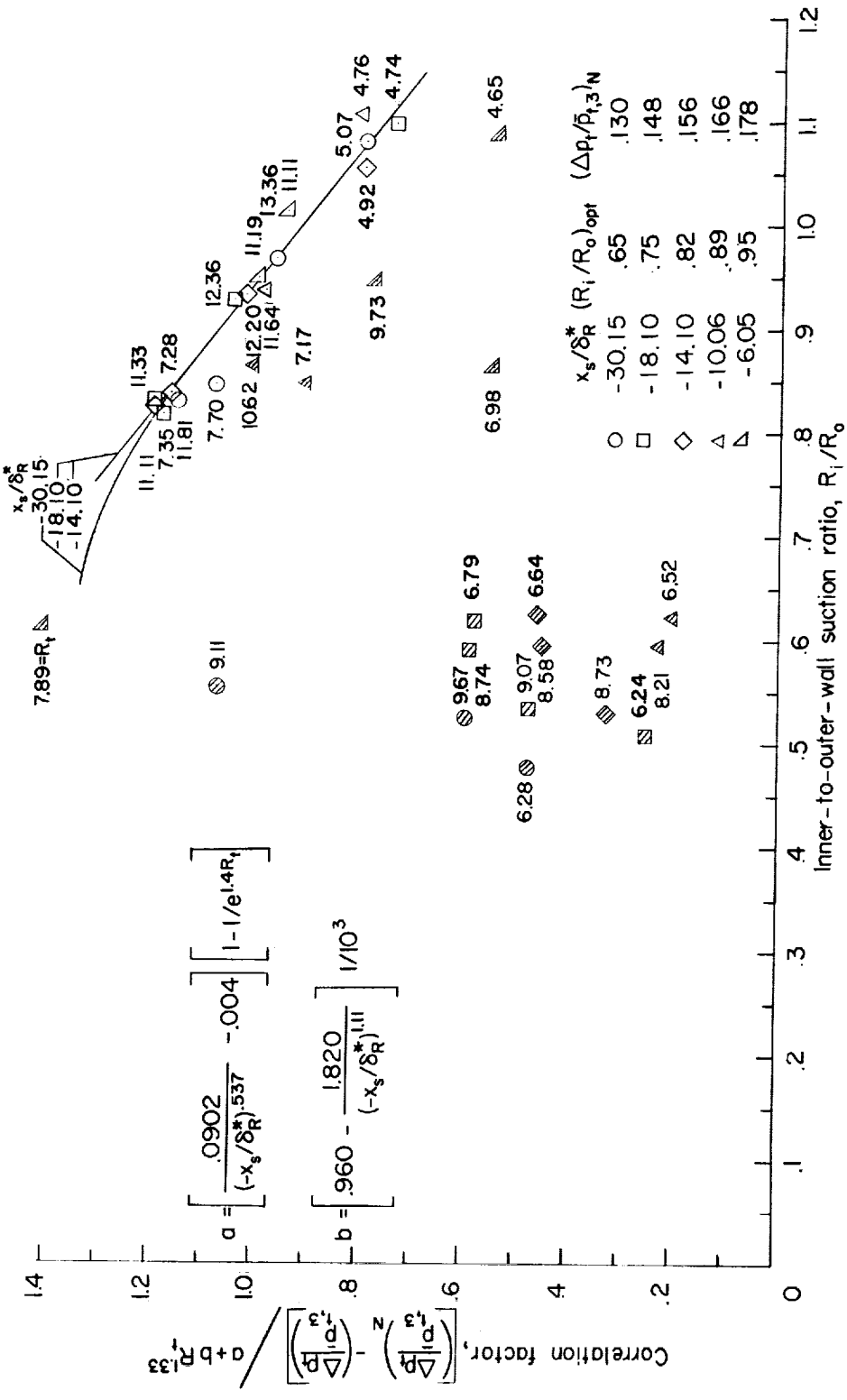

(c) Eight suction rows.

Figure 20.- Concluded.

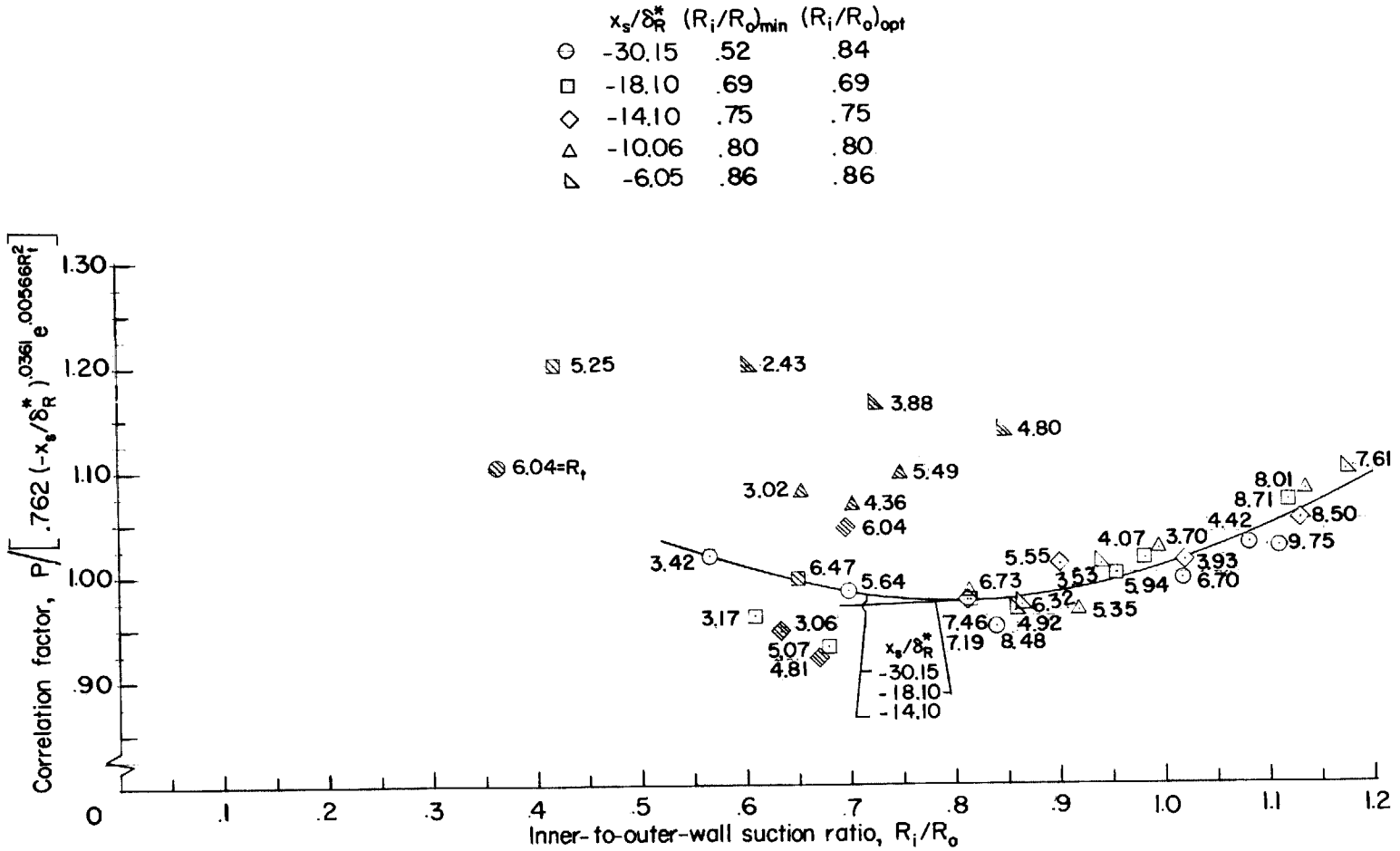

(a) Four suction rows.

Figure 21.- Net pumping-power correlation factor for various inner-to-outer-wall suction ratios. Shaded symbols denote separated flow; numerals indicate values of R_t.

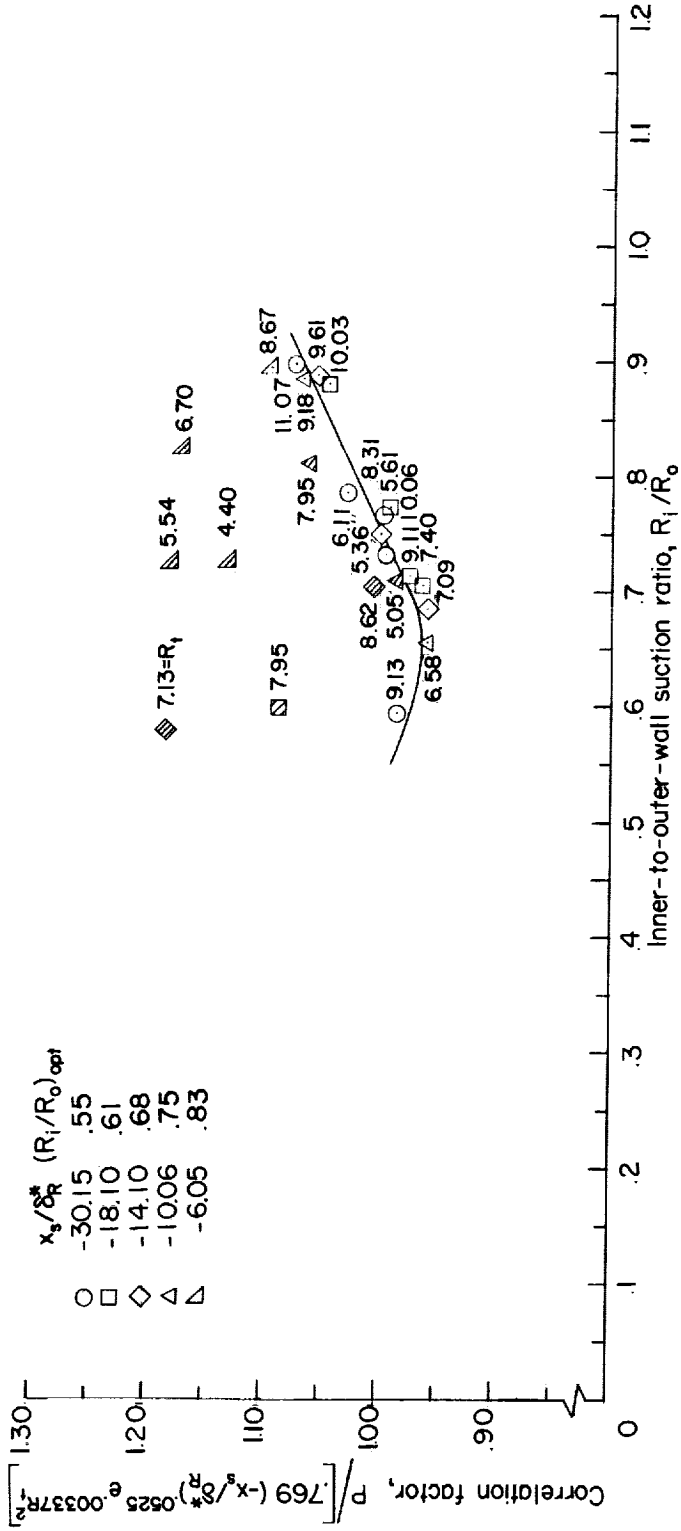

(b) Six suction rows.

Figure 21.- Continued.

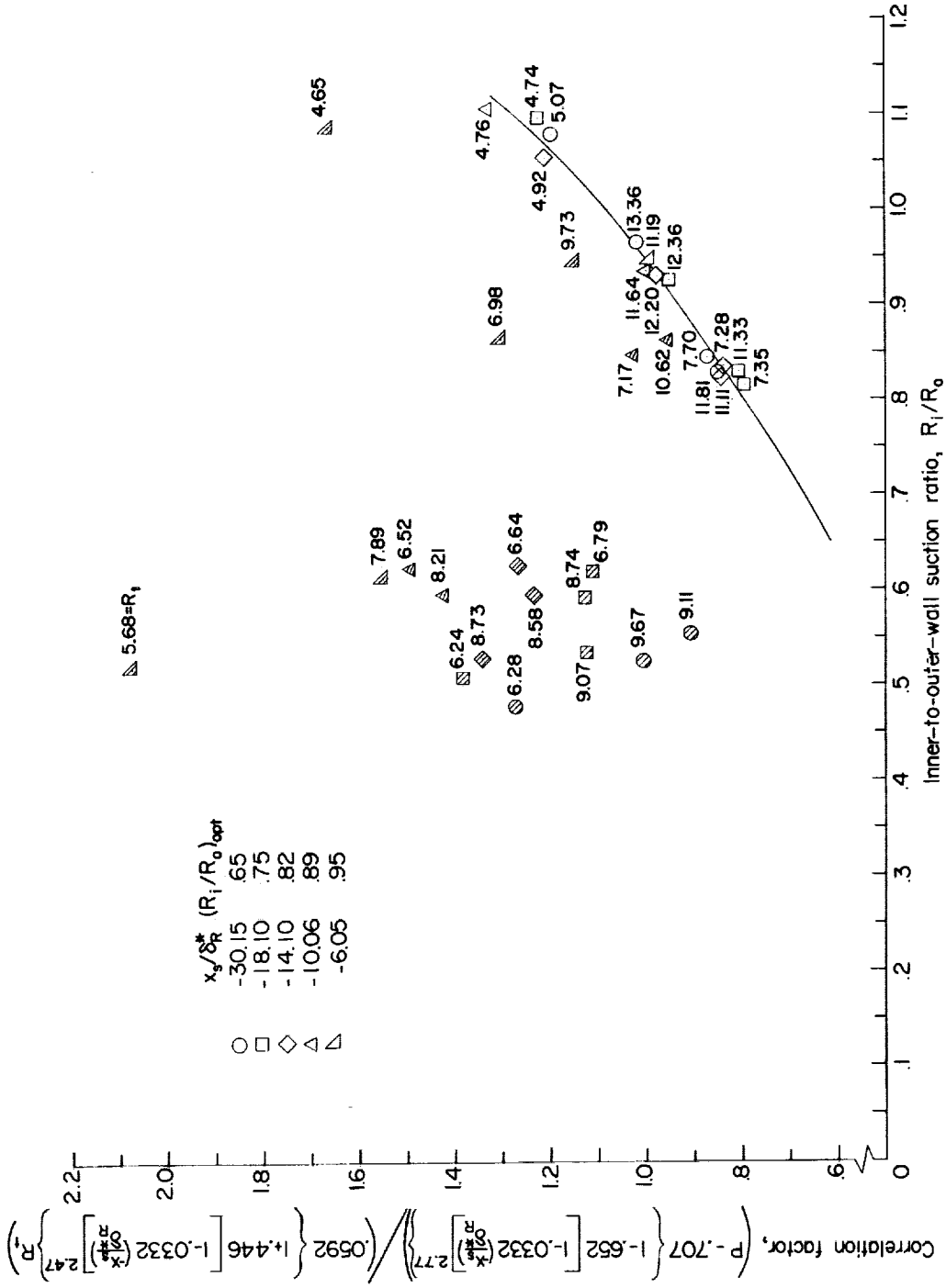

(c) Eight suction rows.

Figure 21.- Concluded.

L-419

NASA TN D-1241
National Aeronautics and Space Administration.
EFFECTS OF SUCTION BOUNDARY-LAYER CONTROL ON THE PERFORMANCE OF A SHORT ANNULAR DIFFUSER WITH AN UPSTREAM TERMINAL NORMAL SHOCK. Charles J. Shoemaker and John R. Henry. April 1962. 59p. OTS price, $1.50. (NASA TECHNICAL NOTE D-1241)

A normal shock was positioned at distances ranging from 0.4 to 2.0 annulus gaps upstream from the diffuser entrance; the corresponding shock Mach number ranged from 1.40 to 1.47. Boundary-layer suction flows as high as about 13 percent of the diffuser entrance flow were employed. The equivalent conical expansion angle of the diffuser was 10°. With about 5-percent suction flow, the over-all total pressure loss of the 10° diffuser was less than that for a 5° diffuser with no boundary-layer control. Pumping-power considerations indicated that suction-flow rates from 5 to 8 percent were economical relative to improved diffuser performance.
Copies obtainable from NASA, Washington

I. Shoemaker, Charles J.
II. Henry, John R.
III. NASA TN D-1241

(Initial NASA distribution:
1, Aerodynamics, aircraft;
37, Propulsion system elements;
38, Propulsion systems, air-jet.)

NASA

NASA TN D-1241
National Aeronautics and Space Administration.
EFFECTS OF SUCTION BOUNDARY-LAYER CONTROL ON THE PERFORMANCE OF A SHORT ANNULAR DIFFUSER WITH AN UPSTREAM TERMINAL NORMAL SHOCK. Charles J. Shoemaker and John R. Henry. April 1962. 59p. OTS price, $1.50. (NASA TECHNICAL NOTE D-1241)

A normal shock was positioned at distances ranging from 0.4 to 2.0 annulus gaps upstream from the diffuser entrance; the corresponding shock Mach number ranged from 1.40 to 1.47. Boundary-layer suction flows as high as about 13 percent of the diffuser entrance flow were employed. The equivalent conical expansion angle of the diffuser was 10°. With about 5-percent suction flow, the over-all total pressure loss of the 10° diffuser was less than that for a 5° diffuser with no boundary-layer control. Pumping-power considerations indicated that suction-flow rates from 5 to 8 percent were economical relative to improved diffuser performance.
Copies obtainable from NASA, Washington

I. Shoemaker, Charles J.
II. Henry, John R.
III. NASA TN D-1241

(Initial NASA distribution:
1, Aerodynamics, aircraft;
37, Propulsion system elements;
38, Propulsion systems, air-jet.)

NASA

NASA TN D-1241
National Aeronautics and Space Administration.
EFFECTS OF SUCTION BOUNDARY-LAYER CONTROL ON THE PERFORMANCE OF A SHORT ANNULAR DIFFUSER WITH AN UPSTREAM TERMINAL NORMAL SHOCK. Charles J. Shoemaker and John R. Henry. April 1962. 59p. OTS price, $1.50. (NASA TECHNICAL NOTE D-1241)

A normal shock was positioned at distances ranging from 0.4 to 2.0 annulus gaps upstream from the diffuser entrance; the corresponding shock Mach number ranged from 1.40 to 1.47. Boundary-layer suction flows as high as about 13 percent of the diffuser entrance flow were employed. The equivalent conical expansion angle of the diffuser was 10°. With about 5-percent suction flow, the over-all total pressure loss of the 10° diffuser was less than that for a 5° diffuser with no boundary-layer control. Pumping-power considerations indicated that suction-flow rates from 5 to 8 percent were economical relative to improved diffuser performance.
Copies obtainable from NASA, Washington

I. Shoemaker, Charles J.
II. Henry, John R.
III. NASA TN D-1241

(Initial NASA distribution:
1, Aerodynamics, aircraft;
37, Propulsion system elements;
38, Propulsion systems, air-jet.)

NASA

NASA TN D-1241
National Aeronautics and Space Administration.
EFFECTS OF SUCTION BOUNDARY-LAYER CONTROL ON THE PERFORMANCE OF A SHORT ANNULAR DIFFUSER WITH AN UPSTREAM TERMINAL NORMAL SHOCK. Charles J. Shoemaker and John R. Henry. April 1962. 59p. OTS price, $1.50. (NASA TECHNICAL NOTE D-1241)

A normal shock was positioned at distances ranging from 0.4 to 2.0 annulus gaps upstream from the diffuser entrance; the corresponding shock Mach number ranged from 1.40 to 1.47. Boundary-layer suction flows as high as about 13 percent of the diffuser entrance flow were employed. The equivalent conical expansion angle of the diffuser was 10°. With about 5-percent suction flow, the over-all total pressure loss of the 10° diffuser was less than that for a 5° diffuser with no boundary-layer control. Pumping-power considerations indicated that suction-flow rates from 5 to 8 percent were economical relative to improved diffuser performance.
Copies obtainable from NASA, Washington

I. Shoemaker, Charles J.
II. Henry, John R.
III. NASA TN D-1241

(Initial NASA distribution:
1, Aerodynamics, aircraft;
37, Propulsion system elements;
38, Propulsion systems, air-jet.)

NASA